Supplementary Information for

Reactivity of Low-valent Nickel Carbonyl Species Supported by Acridane Based PNP Ligands towards Iodoalkanes

Sanha Park,[a] Mi Sook Seo,[a] Mingi Kim,[b] Kang Mun Lee,[b] Peter M. Graham*[c] and Yunho Lee*[a]

a. Department of Chemistry, Seoul National University, Seoul 08826, Republic of Korea. E-mail: yunhochem@snu.ac.kr; Tel: +82 2 880 6653
b. Department of Chemistry, Kangwon National University, Chuncheon 24341, Republic of Korea.
c. Department of Chemistry, Saint Joseph's University, 5600 City Avenue, Philadelphia, PA 19131

Contents

Experimental Section
Figure S1. ^{1}H NMR spectrum of (^{acri}PNP-Ph)Li(THF) in C_6D_6
Figure S2. ^{31}P NMR spectrum of (^{acri}PNP-Ph)Li(THF) in C_6D_6
Figure S3. ^{13}C NMR spectrum of (^{acri}PNP-Ph)Li(THF) in C_6D_6
Figure S4. ^{1}H NMR spectrum of (^{acri}PNP-Ph)Ni–Br in C_6D_6
Figure S5. ^{31}P NMR spectrum of (^{acri}PNP-Ph)Ni–Br in C_6D_6
Figure S6. ^{13}C NMR spectrum of (^{acri}PNP-Ph)Ni–Br in C_6D_6
Figure S7. ^{1}H NMR spectrum of **1**•$C_{10}H_8$ in C_6D_6
Figure S8. ^{1}H NMR spectrum of **2** in C_6D_6
Figure S9. ^{1}H NMR spectrum of **3** in THF-d_8
Figure S10. ^{31}P NMR spectrum of **3** in THF-d_8
Figure S11. ^{13}C NMR spectrum of **3** in THF-d_8
Figure S12. ^{31}P NMR spectrum of **3**•(12-C-4)$_2$ in THF/C_6D_6
Figure S13. ^{1}H NMR spectrum of **4** in C_6D_6
Figure S14. ^{31}P NMR spectrum of **4** in C_6D_6
Figure S15. ^{13}C NMR spectrum of **4** in C_6D_6
Figure S16. ^{1}H NMR spectrum of **5** in C_6D_6
Figure S17. ^{31}P NMR spectrum of **5** in C_6D_6
Figure S18. ^{13}C NMR spectrum of **5** in C_6D_6
Figure S19. ^{1}H NMR spectrum of **5'** in acetone-d_6
Figure S20. ^{13}C NMR spectrum of **5'** in C_6D_6
Figure S21. ^{31}P NMR spectrum of **5'** in C_6D_6
Figure S22. ^{31}P NMR spectra of the reactions of **2** with MeI at –35 °C
Figure S23. ^{31}P NMR spectra of the reactions of **2** with MeI at RT
Figure S24. ^{31}P NMR spectra of the reactions of **2'** with MeI at –35 °C
Figure S25. ^{31}P NMR spectra of the reactions of **2'** with MeI at RT
Figure S26. ^{31}P NMR spectra of the reactions of **3** with MeI at –35 °C
Figure S27. ^{31}P NMR spectra of the reactions of **3** with MeI at RT
Figure S28. ^{31}P NMR spectra of the reactions of **3'** with MeI at –35 °C
Figure S29. ^{31}P NMR spectra of the reactions of **3'** with MeI at RT
Figure S30. ^{31}P NMR spectra of the reactions of **3** with EtI at –35 °C

Figure S31. ^{31}P NMR spectra of the reactions of **3** with EtI at RT
Figure S32. ^{31}P NMR spectra of the reactions of **3'** with EtI at –35 °C
Figure S33. ^{31}P NMR spectra of the reactions of **3'** with EtI at RT
Figure S34. ^{31}P NMR spectra of the reactions of **3** with ^{t}BuI at –35 °C
Figure S35. ^{31}P NMR spectra of the reactions of **3'** with ^{t}BuI at –35 °C
Figure S36. X-Band EPR spectrum of **1** · $C_{10}H_8$ in toluene at 20K
Figure S37. X-Band EPR spectrum of **2** in toluene at 20K
Figure S38. Solid-state structure of (^{acri}PNP-Ph)Ni–Br
Table S1. Selected bond distances and angles of (^{acri}PNP-Ph)Ni–Br
Figure S39. Solid-state structure of **1**
Table S2. Selected bond distances and angles of **1**
Figure S40. Solid-state structure of **2**
Table S3. Selected bond distances and angles of **2**
Figure S41. Solid-state structure of (**3**•(12-C-4)$_2$)
Table S4. Selected bond distances and angles of (**3**•(12-C-4)$_2$)
Figure S42. UV-Vis spectra of (^{acri}PNP-Ph)Ni(Br), **1** · $C_{10}H_8$, **2** and **3**
Figure S43. Cyclic voltammogram of **2**
Figure S44. IR spectra of of (^{acri}PNP-Ph)Ni–Br, **1** · $C_{10}H_8$, **2** and **3**
Figure S45. IR spectrum of of **5**
Figure S46. IR spectrum of of **5'**
Figure S47. Space filling models of [(PNP)Ni–CO]$^-$, [(^{acri}PNP-Ph)Ni–CO]$^-$ (**3**), [(^{acri}PNP-Me)Ni–CO]$^-$ (**3'**)
Figure S48. Buried volumes (V_{bur}) and *G*-parameters of (PNP)Ni–CO, **2** and **2'**
Figure S49. Buried volumes (V_{bur}) and *G*-parameters of anionic portions of [Na][(PNP)Ni–CO], **3** and **3'**
Figure S50. ESI-MS spectrum of **4**
Figure S51. ESI-MS spectrum of **5'**
Figure S52. ESI-MS spectrum of the reaction solution of **3** and EtI under N_2
Figure S53. ESI-MS spectrum of the reaction solution of **3** and ^{t}BuI under N_2
Figure S54. ESI-MS spectrum of the reaction solution of **3'** and EtI under N_2
Figure S55. ESI-MS spectrum of the reaction solution of **3'** and ^{t}BuI under N_2
Table S5. Mulliken spin density of (PNP)Ni–CO, **2** and **2'**
Figure S56. DFT calculated SOMO of (PNP)Ni–CO, **2** and **2'**.
Figure S57. DFT calculated HOMO of [(PNP)Ni–CO]$^-$, [(^{acri}PNP-Ph)Ni–CO]$^-$ (**3**), [(^{acri}PNP-Me)Ni–CO]$^-$ (**3'**).
Cartesian Coordinates
References

EXPERIMENTAL SECTION

General Considerations. All manipulations were carried out using standard Schlenk or glovebox techniques under a N_2 or Ar atmosphere. Solvents were deoxygenated and dried by thoroughly sparging with Ar gas followed by passage through an activated alumina column. Solvents were tested with a standard purple solution of sodium benzophenone ketyl in tetrahydrofuran in order to confirm effective oxygen and moisture removal. All reagents were purchased from commercial vendors and used without further purification unless otherwise stated. 2,7-dimethyl-9,9-diphenyl-9,10-dihydroacridine, complex **2'**, **3'** and **4'** were prepared according to previous literature procedure.[1,2,3] Elemental analyses were carried out at Sogang Center for Research Facilities on Thermo Scientific FLASH 2000 series instrument.

X-ray Crystallography. The diffraction data of complexes were collected on a Bruker D8 QUEST. A suitable size and quality of crystal was coated with Paratone-*N* oil and mounted on a Dual-Thickness MicroLoops LD purchased from MiTeGen. The data were collected with graphite-monochromated MoKα radiation (λ = 0.71073 Å) under a stream of N_2(g) at 100 K. The structures were solved by direct methods, and all non-hydrogen atoms were subjected to anisotropic refinement by full-matrix least squares on F^2 by using the SHELXTL/PC package.[4] Hydrogen atoms were placed at their geometrically calculated positions and refined riding on the corresponding carbon atoms with isotropic thermal parameters. Full crystallographic details can be obtained free of charge from the Cambridge Crystallographic Data Center via (CCDC 2322208, 2281089, 2322241 and 2322236 for (^{acri}PNP-Ph)Ni–Br, **1**, **2** and **3**•(12-C-4)$_2$, respectively.

Spectroscopic Measurements. An Agilent 400-MR and AS500 (Varian) spectrometers were used to measure ^{1}H, ^{31}P and ^{13}C NMR spectra. Deuterated solvents were purchased from Deutero and Euriso-top, degassed, and dried over activated 4-Å molecular sieves prior to use. The chemical shifts for ^{1}H NMR and ^{13}C NMR spectra are quoted in parts per million (ppm) and are referenced to residual solvent peaks. The chemical shifts for ^{31}P spectra are quoted in parts per million (ppm) and are referenced to external phosphoric acid in D_2O at 0.00 ppm. ^{31}P NMR spectra were decoupled by broad band proton decoupling. For measuring the products ratio among **4** (**4'**), **5** (**5'**) and **6** (**6'**), ^{31}P single-pulse NMR spectrum with continuous wave ^{1}H decoupling was acquired employing a 45° excitation pulse of 4 μs and recycle delay of 25 s, which ensured full return of the ^{31}P magnetization to equilibrium in the sample. The following abbreviations were used to describe peak splitting patterns when appropriate: s = singlet, d = doublet, t = triplet, br = broad singlet, m = multiplet, dd = doublet of doublets, td = triplet of doublets, dt = doublet of triplet, ddd = doublet of doublet of doublet, dsep = doublet of septet. Coupling constants, *J*, were reported in hertz unit (Hz). UV–vis spectra were measured by an Agilent Cary 60 UV–vis spectrophotometer using a 1 cm two-window quartz spectrophotometer cell sealed with a screw-cap purchased from Hellma Analytics (117.100-QS). Infrared spectra were recorded in KBr pellets by Bruker Alpha II instrument. Frequencies are given in reciprocal centimeters (cm^{-1}) and only selected absorbances were reported. Electrospray ionization mass (ESI-MS) spectra were obtained by Thermo Scientific LTQ XL linear ion trap mass spectrometer (USA). All sample solutions were directly infused into the mass analyzer using a syringe pump. The temperature of the MS capillary inlet was set to 250 °C and the tube lens voltage was set at 4.5 kV. All EPR measurements were carried out at Korea Basic Science Institute (KBSI) in Seoul, Korea. CW X-band EPR spectra of **1** and **2** were collected on a Bruker EMX plus 6/1

spectrometer equipped with an Oxford Instrument ESR900 liquid He cryostat using an Oxford ITC 503 temperature controller. Spectra were collected with the following experimental parameters: microwave frequency, 9.6 GHz; microwave power, 0.36 mW; modulation amplitude, 10 G; modulation frequency, 100 kHz; temperature, 20 K. The CW-EPR simulations were performed using EasySpin.[5]

Computational Details. The initial geometries for the computational models were obtained from the corresponding X-ray crystal structures. Density functional theory[6] (DFT) geometry optimization and frequency calculations were performed with the B3LYP functional and Def2-SVP basis-set,[7,8] using the Gaussian 16 package.[9] Optimized structures were verified using frequency calculations to confirm the absence of any imaginary frequency. The solvent (tetrahydrofuran) effects were included using the CPCM model.[10] All the Mulliken spin density distribution values are from UB3LYP/Def2-TZVPP//UB3LYP/Def2-SVP. Buried volume calculations were performed using the SambVca 2.1A web application with the use of a 5 Å sphere.[11,13] *G*-parameter calculations were performed using the *solid-G* software.[12,13]

Synthesis of (^{acri}PNP-Ph)Li(THF). To a solution of 4,5-dibromo-2,7-dimethyl-9,9-diphenyl-9,10-dihydroacridine (2.076 g, 4 mmol) in 180 mL diethyl ether, nBuLi (7.5 mL, 1.6 M in hexane, 12 mmol) was slowly added at –78 °C. The reaction mixture was stirred at room temperature for 3 hrs, then it was cooled to –78 °C. Diisopropylchlorophosphine (1.27 g, 8 mmol) was added to the reaction mixture and the resulting solution was stirred at room temperature for 18 hrs. After volatiles were removed in vacuum, the residue was dissolved in benzene. The solution was filtered through Celite. 5 mL THF was added and stirred for 30 min. The volatiles were removed under vacuum. The resulting product (^{acri}PNP-Ph)Li(THF) (1.07 g, 1.60 mmol, 40%) was isolated as a yellow solid after washing with cold pentane and drying under vacuum. ^{1}H NMR (400 MHz, C_6D_6) δ 7.38 (d, *J* = 7.8 Hz, 4H), 7.05 (t, *J* = 7.5 Hz, 6H), 7.00 – 6.94 (m, 4H), 3.10 (s, 4H), 2.25 (s, 6H), 2.03 (q, *J* = 6.7 Hz, 4H), 1.24 (s, 4H), 1.15 (dd, *J* = 14.2, 6.9 Hz, 12H), 1.02 (dd, *J* = 13.4, 7.0 Hz, 12H). ^{13}C NMR (101 MHz, C_6D_6) δ 155.55 (*d*, *J* = 19.2 Hz, Ar-*C*), 150.26 (Ar-*C*), 132.93 (Ar-*C*), 131.45 (Ar-*C*), 130.73 (*d*, Ar-*C*), 129.07 (*d*, Ar-*C*), 127.33 (Ar-*C*), 125.66 (Ar-*C*), 122.14 (*d*, Ar-*C*), 118.25 (Ar-*C*), 118.16 (Ar-*C*), 67.84 (THF), 58.79 (Ar_4-*C*), 25.52 (THF), 24.32 (*C*H(CH_3)$_2$), 21.39 (Ar-*C*H_3), 20.83 (CH(*C*H_3)$_2$), 20.68 (CH(*C*H_3)$_2$), 20.64 (CH(*C*H_3)$_2$), 20.53 (CH(*C*H_3)$_2$). ^{31}P NMR (162 MHz, C_6D_6) δ –4.58 (q, *J* = 51.8 Hz). Anal. Calcd. for $C_{43}H_{56}LiNOP_2$: C, 76.88; H, 8.40; N, 2.08. Found: C, 76.85; H, 8.44; N, 2.17.

Synthesis of (^{acri}PNP-Ph)Ni–Br. A mixture of (^{acri}PNP-Ph)Li(THF) (0.455 g, 0.677 mmol) and $NiBr_2$(DME) (0.215 g, 0.677 mmol) in 40 mL THF was stirred at 60 °C for 14 hrs resulting in a color change from yellowish orange to green. After the volatiles were removed under vacuum, the green residue was dissolved in benzene. The resulting solution was filtered through Celite and the volatiles were removed under vacuum. The resulting product (^{acri}PNP-Ph)Ni–Br (0.453 g, 0.621 mmol, 91%) was isolated as a green solid after washing with cold pentane and drying under vacuum. ^{1}H NMR (400 MHz, C_6D_6) δ 7.20 – 7.17 (m, 2H), 7.07 (t, *J* = 7.5 Hz, 5H), 6.99 (t, *J* = 7.2 Hz, 3H), 6.87 (d, *J* = 2.0 Hz, 4H), 2.45 – 2.34 (m, 4H), 2.03 (s, 6H), 1.45 (q, *J* = 7.6 Hz, 12H), 1.19 (q, *J* = 7.3 Hz, 12H). ^{13}C NMR (101 MHz, C_6D_6) δ 157.47 (t, *J* = 14.14 Hz, Ar-*C*), 147.84 (Ar-*C*), 134.37 (Ar-*C*), 130.80 (Ar-*C*), 130.12 (Ar-*C*), 129.60 (t, *J* = 6.06 Hz, Ar-*C*), 128.59 (Ar-*C*), 126.33 (Ar-*C*), 116.62 (t, *J* = 17.17 Hz, Ar-*C*), 57.34 (Ar_4-*C*), 24.94 (t, *J* = 12.12 Hz, Ar-*C*), 20.66 (Ar-*C*H_3), 18.60 (CH(*C*H_3)$_2$), 17.92 (CH(*C*H_3)$_2$). ^{31}P NMR (162 MHz, C_6D_6) δ 44.59 (s). Anal. Calcd. for $C_{39}H_{48}BrNNiP_2$: C, 64.05; H, 6.62; N, 1.92. Found: C, 64.06; H, 6.65;

N, 1.99. UV-vis [THF, nm (L mol^{-1} cm^{-1})]: 325 (19500), 355 (sh, 9300), 390 (4700), 450 (1900). X-ray quality crystals were grown by slow diffusion of pentane into a saturated THF solution of (^{acri}PNP-Ph)Ni–Br.

Synthesis of (^{acri}PNP-Ph)Ni•$C_{10}H_8$ (1•$C_{10}H_8$). After sodium (23 mg, 1 mmol) was added to the solution of naphthalene (25.6 mg, 0.2 mmol) in 5 mL THF, the reaction mixture was stirred for 3 hrs at room temperature. The resulting sodium naphthalide solution was filtered away from remaining sodium and added dropwise to the green solution of (^{acri}PNP-Ph)Ni–Br (146 mg, 0.2 mmol) in 15 mL THF at –35 °C resulting in an immediate color change to reddish brown. The reaction mixture was stirred for 30 min at room temperature and the volatiles were removed under vacuum. After dissolving in benzene/pentane (3/10), the solution was filtered through Celite and volatiles were removed under vacuum. The resulting product (^{acri}PNP-Ph)Ni•$C_{10}H_8$ **(1•**$C_{10}H_8$**)** (110 mg, 0.14 mmol, 70%) was isolated after washing with cold pentane. ^{1}H NMR (400 MHz, C_6D_6) δ 22.93 (br, s), 7.64 (dd, $C_{10}H_8$), 7.25 (dd, $C_{10}H_8$), 6.51(br, s). Anal. Calcd. for $C_{49}H_{56}NNiP_2$: C, 75.49; H, 7.24; N, 1.80. Found: C, 75.50; H, 7.33; N, 1.98. UV-vis [THF, nm (L mol^{-1} cm^{-1})]: 320 (14000), 366 (14770), 407 (7700), 490 (1100). Crystal suitable for X-ray diffraction were obtained from the concentrated pentane solution at –35 °C.

Synthesis of (^{acri}PNP-Ph)Ni–CO (2). In a 50 mL Schlenk tube, the solution of (^{acri}PNP-Ph)Ni•$C_{10}H_8$ (**1•** $C_{10}H_8$) (78 mg, 0.1 mmol) in 10 mL THF was degassed by three freeze-pump-thaw cycles on the Schlenk line. CO(g) was charged under ambient conditions resulting in an immediate color change from red to dark green. The solution was stirred for 10 min, and all volatiles were removed under vacuum. The resulting product (^{acri}PNP)Ni–CO (**2**) (68 mg, 0.085 mmol, 85%) was isolated as a green crystalline solid after recrystallization in diethyl ether at –35 °C. ^{1}H NMR (400 MHz, C_6D_6) δ 7.63 (dd, $C_{10}H_8$), 7.25 (dd, $C_{10}H_8$), 3.58 (br). IR (KBr Pellet, cm^{-1}): ν_{co} 1932. Anal. Calcd. for $C_{40}H_{48}NNiOP_2$: C, 70.71; H, 7.12; N, 2.06. Found: C, 70.35; H, 7.50; N, 2.00. UV-vis [THF, nm (L mol^{-1} cm^{-1})]: 320 (13000), 350 (11000), 480 (1600), 620 (720). Crystal suitable for X-ray diffraction were obtained from the concentrated pentane solution at –35 °C.

Synthesis of {Na}{^{acri}PNP-Ph)Ni–CO} (3). After sodium (40 mg) was added to a solution of naphthalene (22 mg, 0.156 mmol) in 5 mL THF, the reaction mixture was stirred for 3 hrs at room temperature. The resulting sodium naphthalide solution was filtered away from remaining sodium and added dropwise to the green solution of (^{acri}PNP-Ph)Ni–CO (**2**) (106 mg, 0.156 mmol) in 10 mL THF at –35 °C resulting an immediate color change from deep green to deep brown. After stirring for 1 hr the solution was filtered through Celite and the volatiles were removed under vacuum. The resulting product {Na}{^{acri}PNP-Ph)Ni–CO} (**3**) (104 mg, 0.148 mmol, 95%) was isolated as a yellow powder after washing with pentane and drying under vacuum. ^{1}H NMR (400 MHz, THF-d_8) δ 7.18 – 7.15 (m, 6H, Ar-*H*), 7.10 – 7.07 (m, 4H, Ar-*H*), 6.88 (m, 2H, Ar-*H*), 6.33 (s, 2H, Ar-*H*), 2.59 – 2.51 (m, 2H, C*H*$(CH_3)_2$), 2.13 (s, 6H, Ar–CH_3), 1.89 – 1.83 (m, 2H, C*H*$(CH_3)_2$) 1.37 (q, 6H, CH(CH_3)$_2$), 1.21 (q, 6H, CH(CH_3)$_2$), 1.00 (q, 6H, CH(CH_3)$_2$), 0.78 (q, 6H, CH(CH_3)$_2$). ^{13}C NMR (101 MHz, C_6D_6) δ 206.92 (Ni*C*O) 157.47 (t, *J* = 14.14 Hz, Ar-*C*), 149.46 (Ar-*C*), 148.51 (Ar-*C*), 133.15 (Ar-*C*) 132.55 (Ar-*C*), 130.93 (Ar-*C*), 130.08 (Ar-*C*), 129.89 (Ar-*C*), 128.70 (Ar-*C*), 127.77 (Ar-*C*), 126.94 (Ar-*C*), 126.67 (Ar-*C*), 124.15 (Ar-*C*), 59.61 (Ar$_4$(C)) 35.24 (*C*H$(CH_3)_2$), 26.55 (*C*H$(CH_3)_2$), 21.31 (CH(*C*H_3)$_2$), 21.21 (CH(*C*H_3)$_2$), 20.78 (CH(*C*H_3)$_2$), 20.37 (CH(*C*H_3)$_2$). ^{31}P NMR (162 MHz, THF-d_8) δ 54.77 ppm (s). IR (KBr Pellet, cm^{-1}): ν_{co} 1799. Anal. Calcd. for $C_{40}H_{48}NNaNiOP_2$: C, 68.39; H, 6.89; N,

1.99. Found: C, 68.43; H, 6.84; N, 1.89. UV-vis [THF, nm (L mol^{-1} cm^{-1})]: 310 (10500), 350 (10400).

Separate Synthesis of {Na(12-C-4)$_2$}{^{acri}PNP-Ph)Ni–CO} (3•(12-C-4)$_2$) for obtaining crystals suitable for X-ray diffraction. To a solution of {Na}{(^{acri}PNP-Ph)Ni–CO} (**3**) (47.5 mg, 0.068 mmol) in 5 mL THF, 12-crown-4 (22 µL, 0.137 mmol) was added using a microsyringe. The reaction mixture was stirred for 30 min at room temperature. The solution was filtered through Celite and the volatiles were removed under vacuum. The resulting product {Na(12-C-4)$_2$}{^{acri}PNP-Ph)Ni–CO} (**3**•(12-C-4)$_2$) (65 mg, 0.062 mmol, 91%) was isolated as a red powder after washing with pentane and drying under vacuum. ^{31}P NMR (162 MHz, THF/C_6D_6) δ 55.03 (s). Anal. Calcd. for $C_{56}H_{80}NNaNiO_9P_2$: C, 63.76; H, 7.64; N, 1.33. Found: C, 63.64; H, 7.56; N, 1.30. Crystals suitable for X-ray diffraction were grown by slow diffusion of pentane into a saturated THF solution of {Na(12-C-4)$_2$}{^{acri}PNP-Ph)Ni–CO} (**3**•(12-C-4)$_2$) at –35 °C.

Separate synthesis of (^{acri}PNP-Ph)Ni–Me (4). To a solution of (^{acri}PNP-Ph)NiBr (88 mg, 0.12 mmol) in 10 mL THF, MeMgCl (40 µL, 3.0 M in THF, 0.12mmol) was added at room temperature. The reaction mixture was stirred for 2 hrs resulting in a color change from red to dark brown. After adding 1,4-dioxane (20 µL), the reaction mixture was stirred for 30 min and volatiles were removed under vacuum. After the residue was dissolved in benzene, the solution was filtered through Celite and volatiles were removed under vacuum. The resulting product (^{acri}PNP-Ph)Ni–Me (**4**) (73.2 mg, 0.11 mmol, 92%) was isolated as a yellow solid after wash with cold pentane. ^{1}H NMR (400 MHz, C_6D_6) δ 7.29 (d, 4H, *J* = 8.0 Hz, Ar-*H*), 7.09 (t, 4H, *J* = 8.0 Hz, Ar-*H*), 7.01 – 6.96 (m, 4H, Ar-*H*), 6.92 (s, 2H, Ar-*H*), 2.23 – 2.20 (m, 4H, C*H*(CH$_3$)$_2$), 2.12 (s, 6H, Ar–C*H*$_3$), 1.19 (q, 12H, CH(C*H*$_3$)$_2$), 1.13 (q, 12H, CH(C*H*$_3$)$_2$), –0.21 (t, 3H, Ni–C*H*$_3$). ^{13}C NMR (101 MHz, C_6D_6) δ 156.90 (t, *J* = 14.14 Hz, Ar-*C*), 148.57 (Ar-*C*), 133.90 (Ar-*C*), 130.98 (Ar-*C*), 129.91 (Ar-*C*), 128.59 (Ar-*C*), 127.65 (Ar-*C*), 126.02 (Ar-*C*), 124.87 (t, *J* = 3.03 Hz, Ar-*C*), 117.58 (t, *J* = 17.17 Hz, Ar-*C*), 57.74 (Ar$_4$-*C*), 24.20 (t, *J* = 12.12 Hz, *C*H(CH$_3$)), 20.95 (Ar-*C*H$_3$), 18.66 (t, *J* = 3.03 Hz, CH(*C*H$_3$)$_2$), 18.11 (CH(*C*H$_3$)$_2$) –25.38 (t, $^2J_{c\text{-}p}$ = 25.25 Hz, Ni–*C*H$_3$). ^{31}P NMR (162 MHz, C_6D_6) δ 41.25 (s). ESI-MS {(^{acri}PNP-Ph)Ni–Me}$^+$: calcd, 665.29; found, 665.27.

Separate synthesis of (^{acri}PNP-Ph)Ni–COMe (5). In a 50 mL Schlenk tube, **4** (100 mg, 0.150 mmol) was dissolved in 15 mL of benzene. After three freeze-pump-thaw cycles of solution, CO gas was introduced into the Schlenk tube at ambient pressure. The reaction mixture was stirred for 40 hrs at 80 °C. After degassing the solution by freeze-pump-thaw, the solution was filtered through Celite. All volatiles were removed under vacuum. The resulting (^{acri}PNP-Ph)Ni–COMe (**5**) (80 mg, 0.116 mmol, 77%) was isolated as a yellow solid after washing with cold pentane. ^{1}H NMR (400 MHz, C_6D_6) δ 7.29 – 7.26 (m, 4H, Ar-*H*), 7.11 – 7.08 (m, 4H, Ar-*H*), 7.02 (m, 2H, Ar-*H*), 6.90 (s, 2H, Ar-*H*), 6.85 – 6.82 (m, 2H, Ar-*H*), 2.40 (s, 3H, COC*H*$_3$), 2.20 – 2.16 (m, 4H, C*H*(CH$_3$)$_2$), 2.09 (s, 6H, Ar-C*H*$_3$), 1.16–1.12 (m, 24H, CH(C*H*$_3$)$_2$). ^{13}C NMR (101 MHz, C_6D_6) δ 261.67 (t, *J* = 21.2 Hz, Ni*C*OMe), 156.03 (t, *J* = 14.14 Hz, Ar-*C*), 148.30 (Ar-*C*), 134.07 (Ar-*C*), 129.68 (Ar-*C*), 128.80 (Ar-*C*), 128.59 (Ar-*C*), 126.08 (Ar-*C*), 124.99 (t, *J* = 3.03 Hz, Ar-*C*), 115.48 (t, *J* = 19.2 Hz, Ar-*C*), 57.67 (Ar$_4$-*C*), 42.76 (s, CO*C*H$_3$) 23.20 (*C*H(CH$_3$)$_2$), 20.93 (Ar-*C*H$_3$), 18.22 (CH(*C*H$_3$)$_2$), 17.38 (CH(*C*H$_3$)$_2$). ^{31}P NMR (162 MHz, C_6D_6) δ 40.00 (s). IR (KBr Pellet, cm^{-1}): ν_{co} 1613. Anal. Calcd. for $C_{41}H_{51}NNiOP_2$: C, 70.91; H, 7.40; N, 2.02. Found: C, 70.96; H, 7.51; N, 2.06.

Separate synthesis of (^{acri}PNP-Me)Ni–COMe (5'). In a 100 mL Schlenk tube, **4'** (313 mg, 0.580 mmol) was dissolved in 15 mL of benzene. After three freeze-pump-thaw cycles of solution, CO gas was introduced into the Schlenk tube at ambient pressure. The reaction mixture was stirred for 36 hrs at 80 °C. After degassing the solution by freeze-pump-thaw, the solution was filtered through Celite. All volatiles were removed under vacuum. The resulting (^{acri}PNP-Me)Ni–COMe (**5'**) (280 mg, 0.490 mmol, 84%) was isolated as a yellow solid after washing with cold pentane. ^{1}H NMR (400 MHz, acetone-d_6) δ 7.35 (s, 1H, Ar-*H*), 7.05 (s, 2H, Ar-*H*), 6.89 (t, 2H, Ar-*H*), 6.92 (s, 2H, Ar-*H*), 2.52 – 2.48 (m, 4H, C*H*(CH_3)$_2$), 2.38 (s, 3H, COC*H*$_3$), 2.20 (s, 6H, Ar-C*H*$_3$), 1.24–1.21 (m, 24H, CH(C*H*$_3$)$_2$). ^{13}C NMR (101 MHz, C_6D_6) δ 262.23 (t, *J* = 20.2 Hz, Ni*C*OMe), 155.42 (t, *J* = 13.13 Hz, Ar-*C*), 130.76 (t, *J* = 5.05 Hz, Ar-*C*), 130.18 (Ar-*C*), 129.43 (Ar-*C*), 124.69 (t, *J* = 3.03 Hz, Ar-*C*), 115.45 (t, *J* = 19.2 Hz, Ar-*C*), 43.39 (t, CO*C*H$_3$), 36.37 (s, Ar$_2$*C*(CH_3)$_2$), 23.67(s, *C*H(CH_3)$_2$), 21.01(s, Ar-*C*H$_3$), 18.03 (s, CH(*C*H$_3$)$_2$) 17.44 (s, CH(*C*H$_3$)$_2$). ^{31}P NMR (162 MHz, C_6D_6) δ 39.35 (s). IR (KBr Pellet, cm^{-1}): ν_{CO} 1602. Anal. Calcd. for $C_{31}H_{47}NNiOP_2$: C, 65.28; H, 8.31; N, 2.46. Found: C, 65.29; H, 8.32; N, 2.41. ESI-MS {(^{acri}PNP-Me)Ni–COMe}$^+$: calcd, 569.25; found, 569.25.

Reaction of 2 with MeI at –35 °C and RT. To a green solution of **2** (16 mg, 0.024 mmol) in 3 mL of THF, MeI (13 μL, 2.0 M in ^{t}BuOMe, 0.026 mmol) was added using a microsyringe at –35 °C or RT resulting in a color change to yellowish green. The reaction mixture was stirred for 30 mins at room temperature and all volatiles were removed under vacuum. The yields of the products were determined by single-pulse ^{31}P NMR spectroscopy. The reaction was done at least three times for reproducibility.

Reaction of 2' with MeI at –35 °C and RT. To a green solution of **2'** (17 mg, 0.025 mmol) in 3 mL of THF, MeI (14 μL, 2.0 M in ^{t}BuOMe, 0.028 mmol) was added using a microsyringe at –35 °C or RT resulting in a color change to yellowish green. The reaction mixture was stirred for 30 mins at room temperature and all volatiles were removed under vacuum. The yields of the products were determined by single-pulse ^{31}P NMR spectroscopy. The reaction was done at least three times for reproducibility.

Reaction of 3 with MeI at –35 °C and RT. To a red solution of **3** (20 mg, 0.028 mmol) in 3 mL of THF, MeI (15 μL, 2.0 M in ^{t}BuOMe, 0.030 mmol) was added using a microsyringe at –35 °C or RT resulting in a color change to yellowish green. The reaction mixture was stirred for 30 mins at room temperature and all volatiles were removed under vacuum after the Celite filtration with benzene. The yields of the products were determined by single-pulse ^{31}P NMR spectroscopy. The reaction was done multiple times for reproducibility.

Reaction of 3' with MeI at –35 °C and RT. To a red solution of **3'** (15 mg, 0.026 mmol) in 3 mL of THF, MeI (14 μL, 2.0 M in ^{t}BuOMe, 0.028 mmol) was added using a microsyringe at –35 °C or RT resulting in a color change to yellowish green. The reaction mixture was stirred for 30 mins at room temperature and all volatiles were removed under vacuum after the Celite filtration with benzene. The yields of the products were determined by single-pulse ^{31}P NMR spectroscopy. The reaction was done multiple times for reproducibility.

Reaction of 3 with EtI at –35 °C and RT. To a red solution of **3** (26 mg, 0.037 mmol) in 4 mL of THF, EtI (3.5 μL, 0.044 mmol) was added using a microsyringe at –35 °C or RT resulting in a color change to yellow. The reaction mixture was stirred for 30 mins at room temperature and all volatiles were removed under vacuum after the Celite filtration with benzene. The yields of the products were determined by single-pulse ^{31}P NMR spectroscopy. The reaction was done multiple times for reproducibility.

Reaction of 3' with EtI at –35 °C and RT. To a red solution of **3'** (21 mg, 0.036 mmol) in 4 mL of THF, EtI (3.4 μL, 0.042 mmol) was added using a microsyringe at –35 °C or RT resulting in a color change to yellow. The reaction mixture was stirred for 30 mins at room temperature and all volatiles were removed under vacuum after the Celite filtration with benzene. The yields of the products were determined by single-pulse ^{31}P NMR spectroscopy. The reaction was done multiple times for reproducibility.

Reaction of 3 with ^{t}BuI at –35 °C and RT. To a red solution of **3** (26 mg, 0.037 mmol) in 4 mL of THF, ^{t}BuI (5.5 μL, 0.044 mmol) was added using a microsyringe at –35 °C or RT resulting in a color change to yellow. The reaction mixture was stirred for 30 mins at room temperature and all volatiles were removed under vacuum after the Celite filtration with benzene. The yields of the products were determined by single-pulse ^{31}P NMR spectroscopy. The reaction was done multiple times for reproducibility.

Reaction of 3' with ^{t}BuI at –35 °C and RT. To a red solution of **3'** (21 mg, 0.036 mmol) in 4 mL of THF, ^{t}BuI (5.5 μL, 0.044 mmol) was added using a microsyringe at –35 °C or RT resulting in a color change to yellow. The reaction mixture was stirred for 30 mins at room temperature and all volatiles were removed under vacuum after the Celite filtration with benzene. The yields of the products were determined by single-pulse ^{31}P NMR spectroscopy. The reaction was done multiple times for reproducibility.

Figure S1. ^{1}H NMR spectrum of (^{acri}PNP-Ph)Li(THF) in C_6D_6 at room temperature.

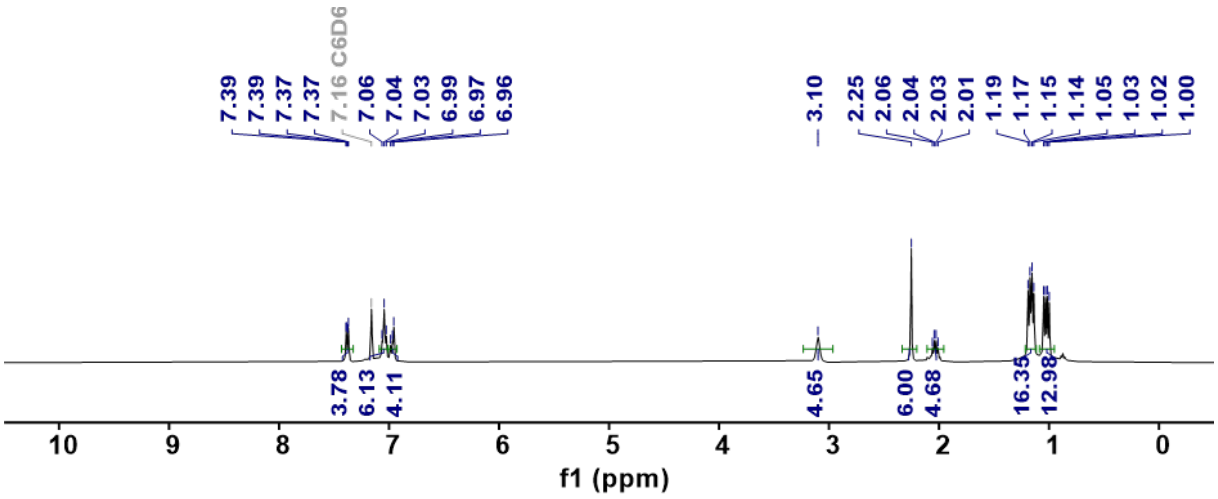

Figure S2. ^{31}P NMR spectrum of (^{acri}PNP-Ph)Li(THF) in C_6D_6 at room temperature.

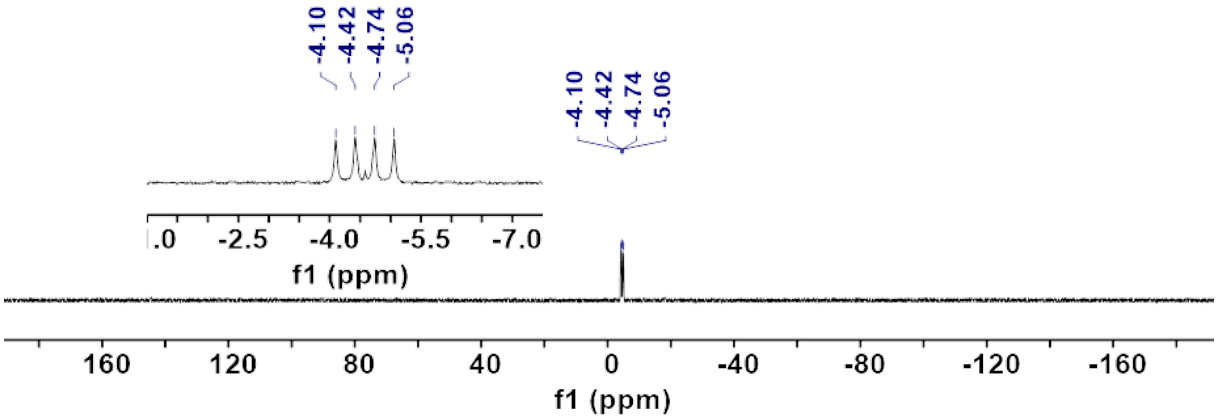

Figure S3. ^{13}C NMR spectrum of (^{acri}PNP-Ph)Li(THF) in C_6D_6 at room temperature (●:pentane).

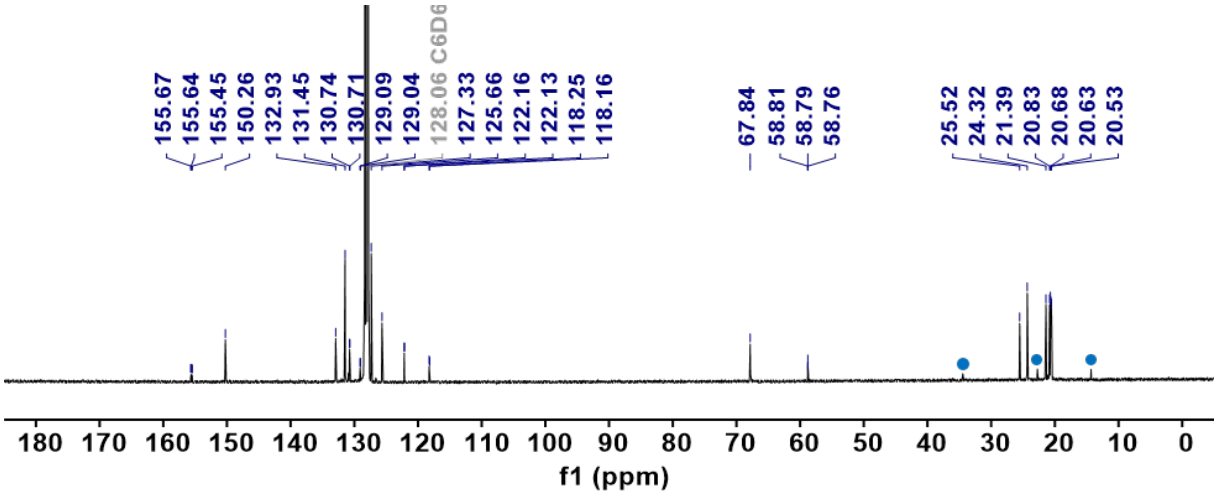

Figure S4. ^{1}H NMR spectrum of (^{acri}PNP-Ph)Ni–Br in C_6D_6 at room temperature.

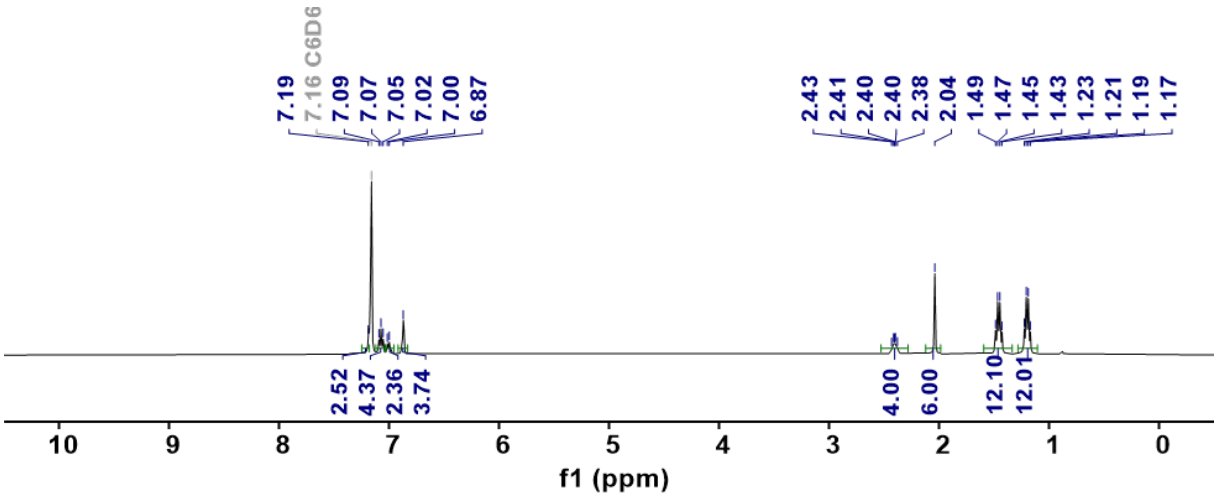

Figure S5. ^{31}P NMR spectrum of (^{acri}PNP-Ph)Ni–Br in C_6D_6 at room temperature.

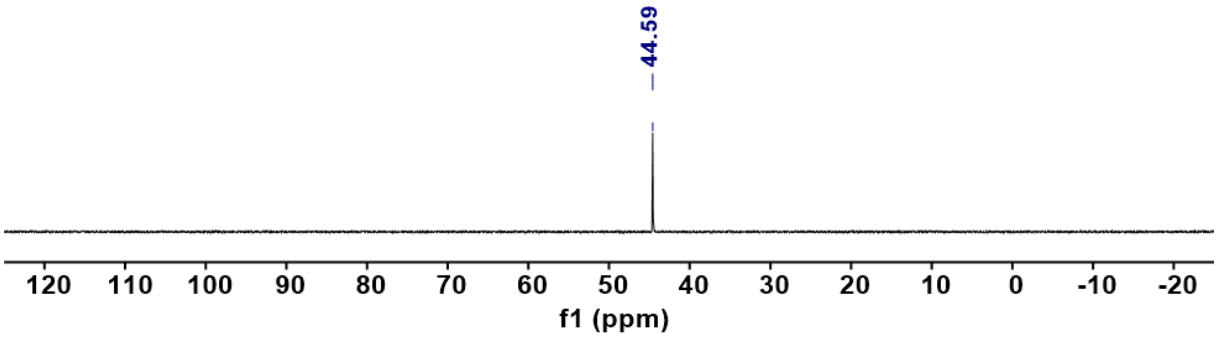

Figure S6. ^{13}C NMR spectrum of (^{acri}PNP-Ph)Ni–Br in C_6D_6 at room temperature.

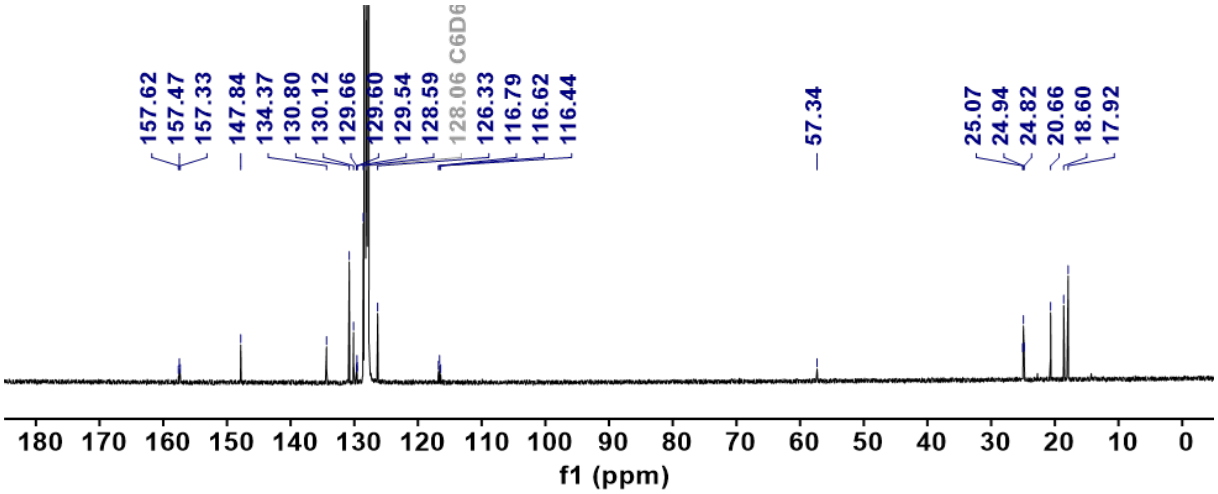

Figure S7. ^{1}H NMR spectrum of (^{acri}PNP-Ph)Ni•$C_{10}H_8$ (**1**•$C_{10}H_8$) in C_6D_6 at room temperature.

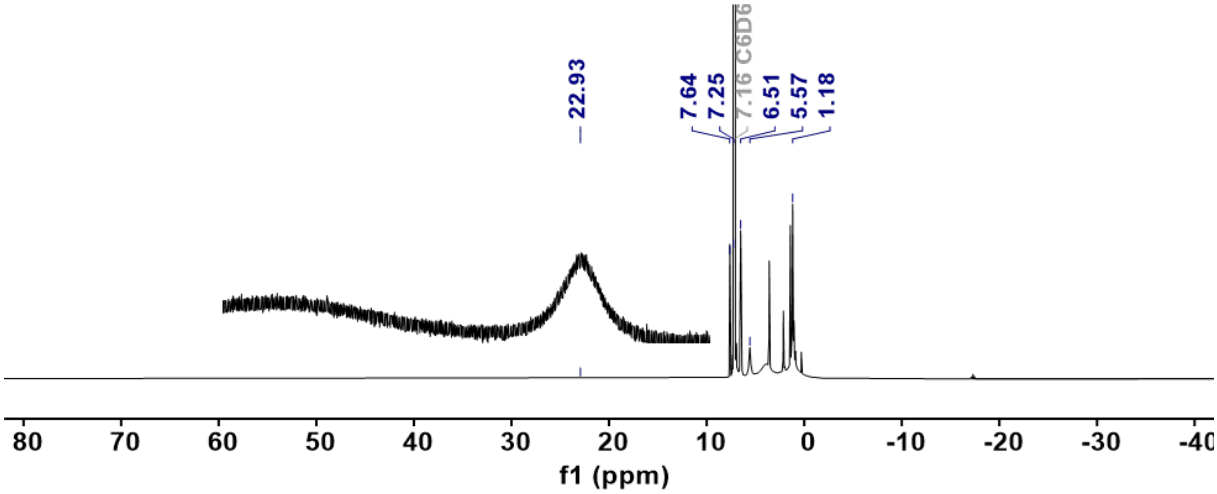

Figure S8. ^{1}H NMR spectrum of (^{acri}PNP-Ph)Ni–CO (**2**) in C_6D_6 at room temperature.

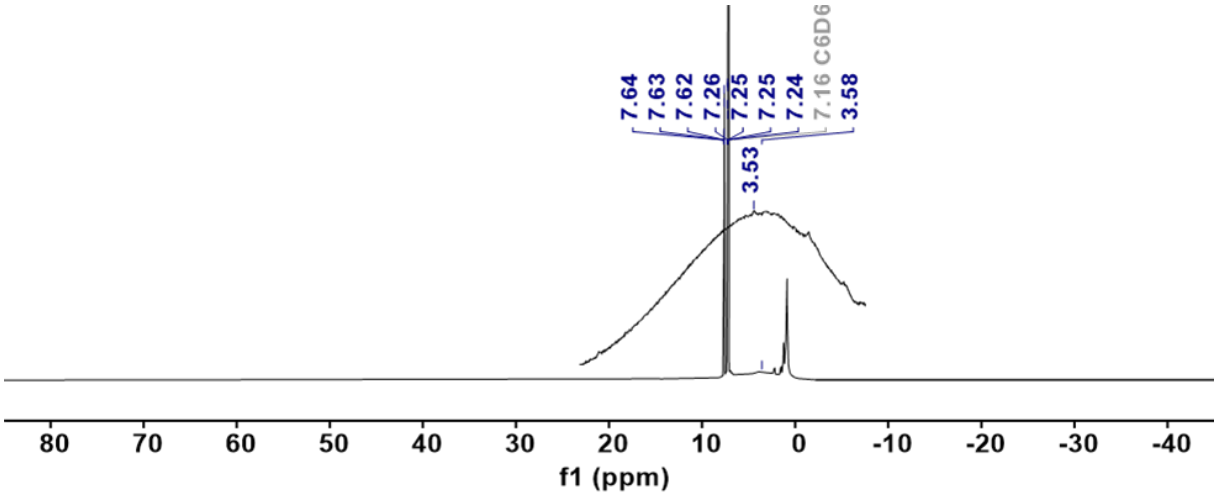

Figure S9. ^{1}H NMR spectrum of {Na}{(^{acri}PNP-Ph)Ni–CO} (**3**) in THF-d_8 at room temperature.

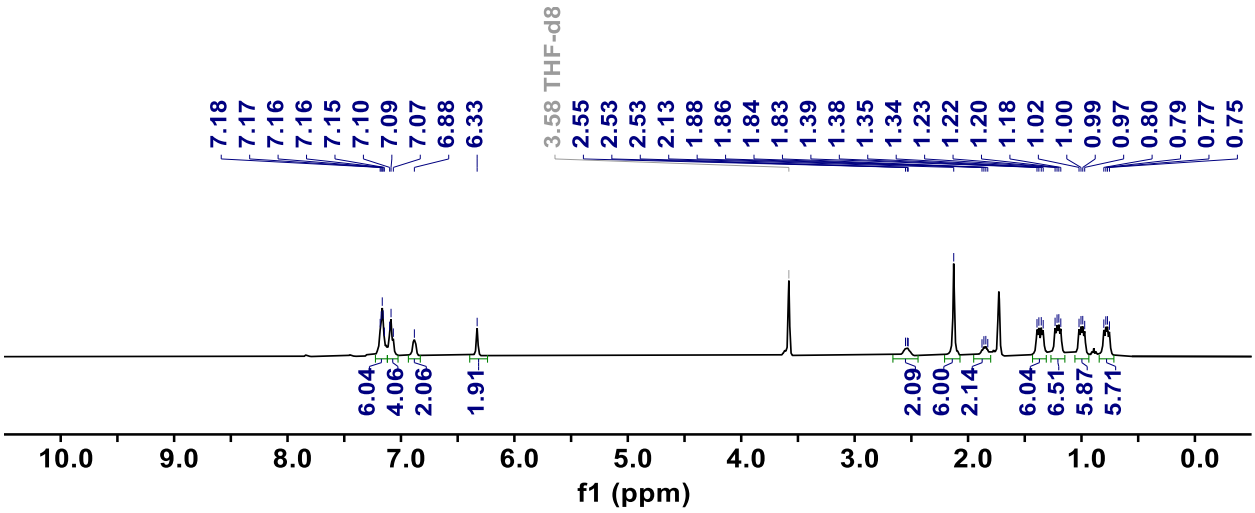

Figure S10. ^{31}P NMR spectrum of {Na}{(^{acri}PNP-Ph)Ni–CO} (**3**) in THF-d_8 at room temperature.

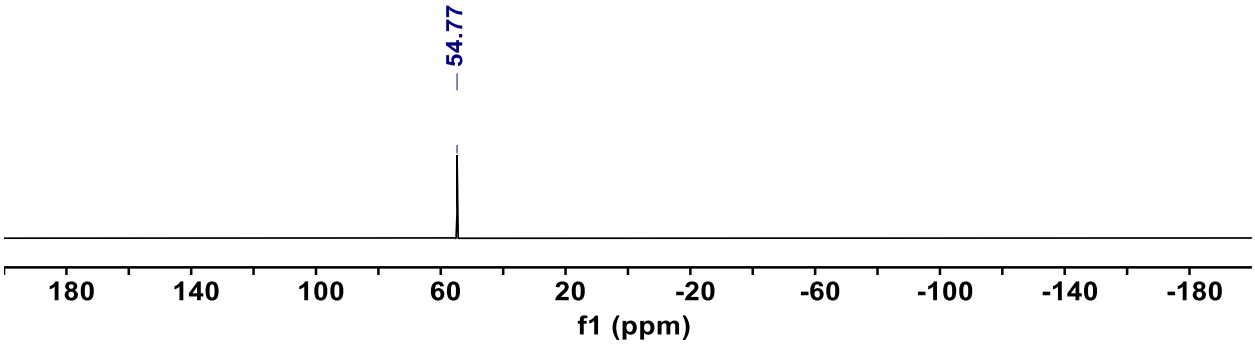

Figure S11. ^{13}C NMR spectrum of {Na}{(^{acri}PNP-Ph)Ni–CO} (**3**) in THF-d_8 at room temperature (●:pentane).

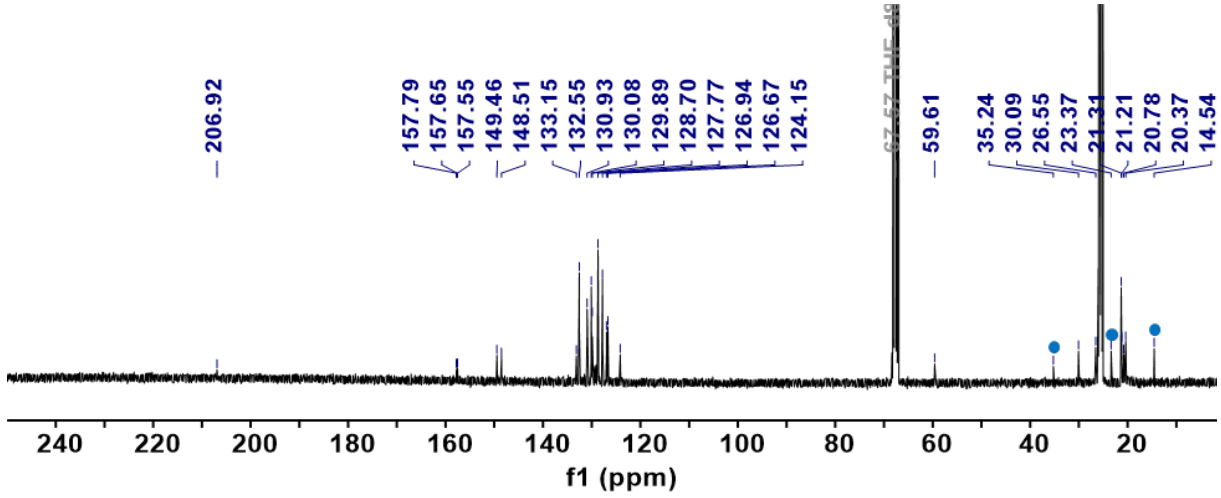

Figure S12. ^{31}P NMR spectrum of {Na(12-C-4)$_2$}{(^{acri}PNP-Ph)Ni–CO} (**3** · (12-C-4)$_2$) in THF/C_6D_6 at room temperature.

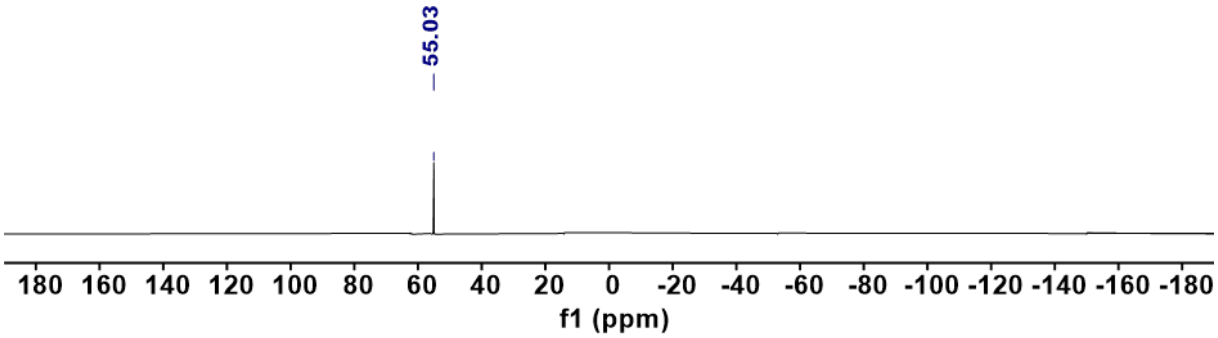

Figure S13. ^{1}H NMR spectrum of (^{acri}PNP-Ph)Ni–Me (**4**) in C_6D_6 at room temperature.

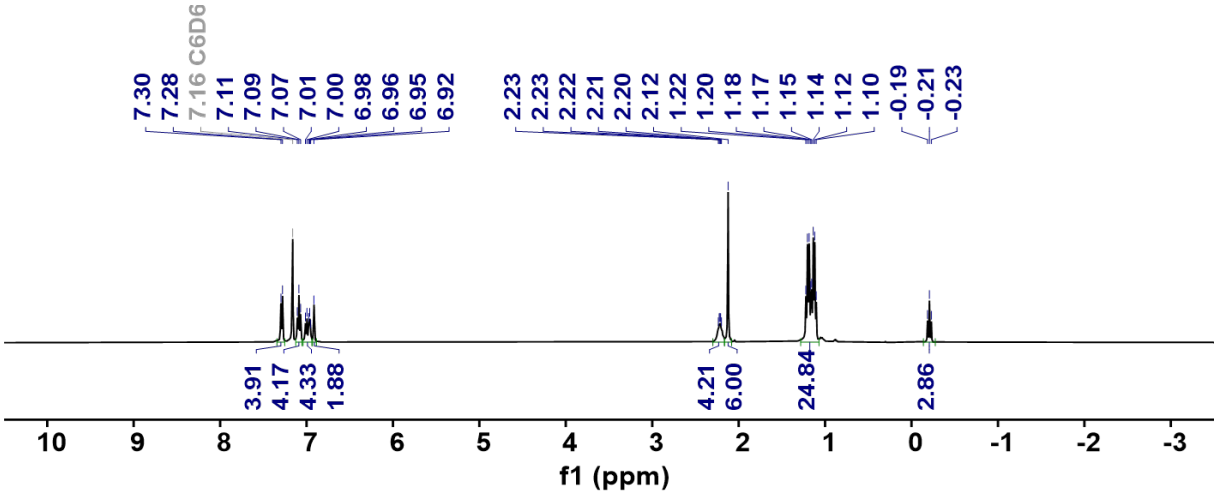

Figure S14. ^{31}P NMR spectrum of (^{acri}PNP-Ph)Ni–Me (**4**) in C_6D_6 at room temperature.

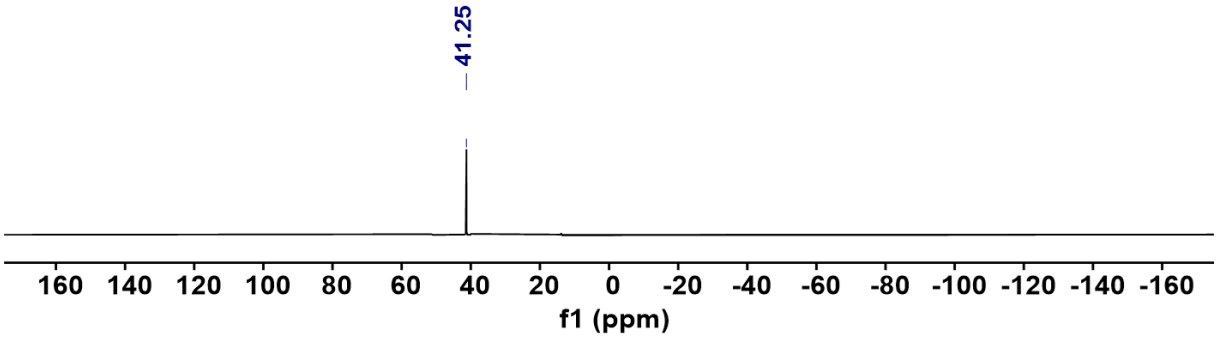

Figure S15. ^{13}C NMR spectrum of (^{acri}PNP-Ph)Ni–Me (**4**) in C_6D_6 at room temperature.

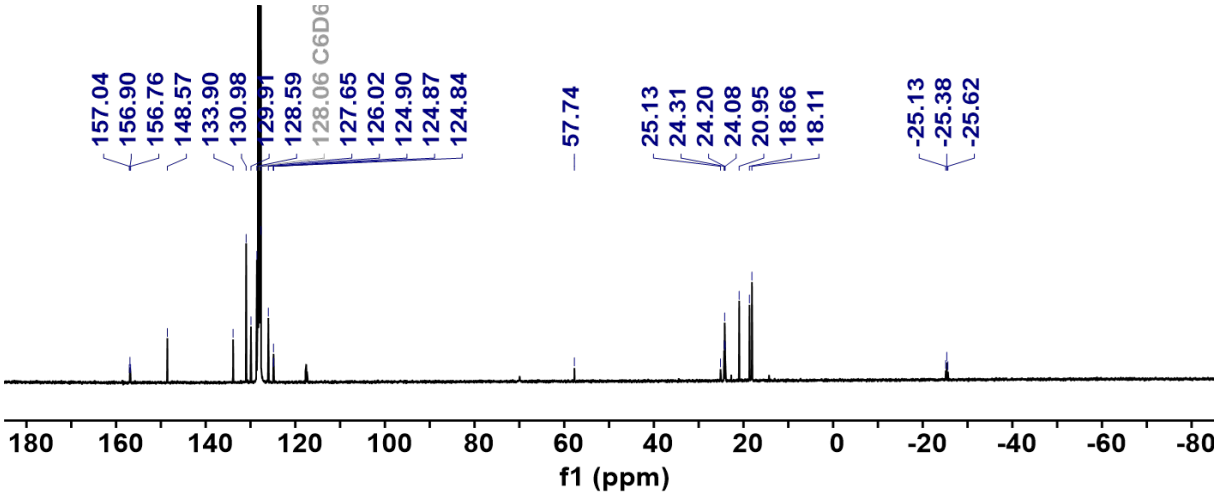

Figure S16. ^{1}H NMR spectrum of (^{acri}PNP-Ph)Ni–COMe (**5**) in C_6D_6 at room temperature.

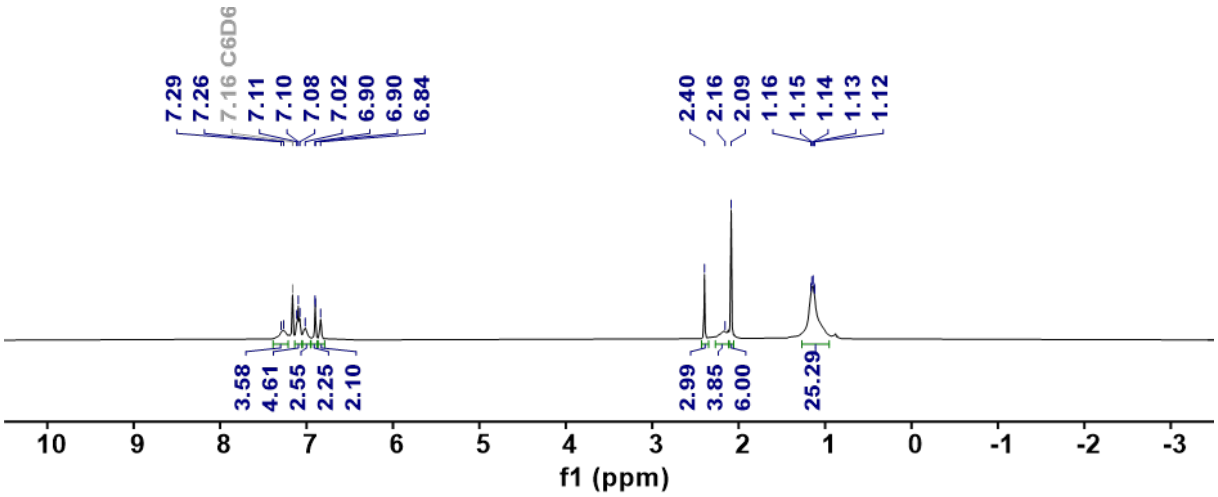

Figure S17. ^{31}P NMR spectrum of (^{acri}PNP-Ph)Ni–COMe (**5**) in C_6D_6 at room temperature.

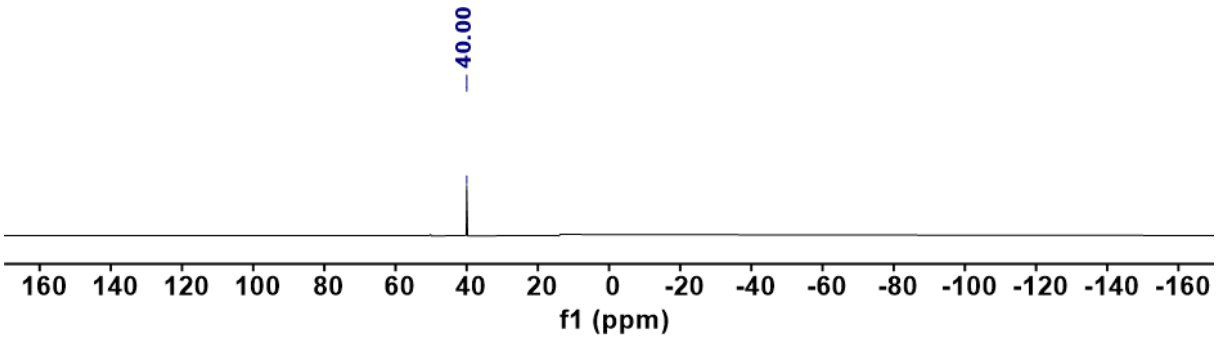

Figure S18. ^{13}C NMR spectrum of (^{acri}PNP-Ph)Ni–COMe (**5**) in C_6D_6 at room temperature.

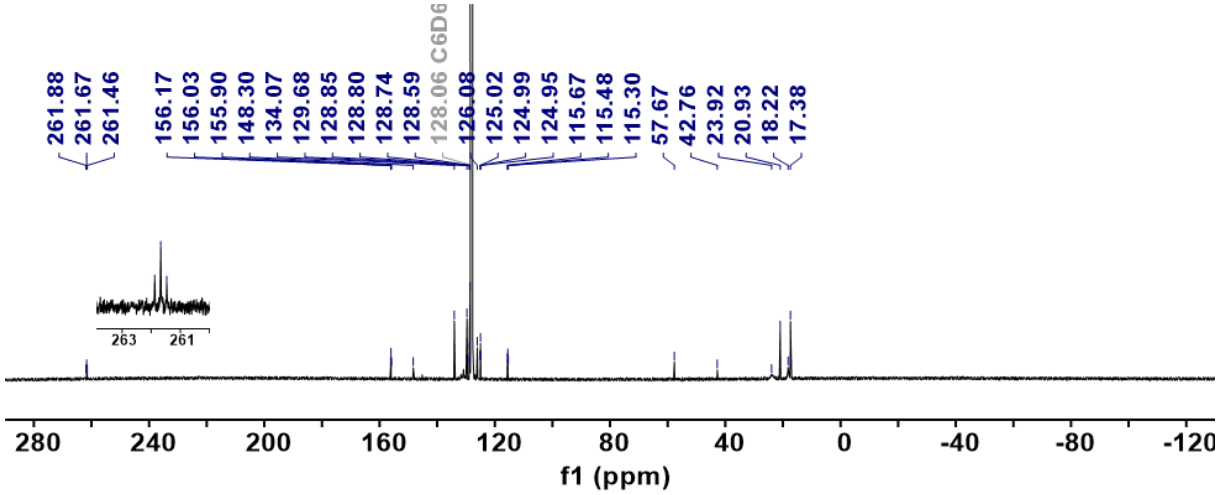

Figure S19. ^{1}H NMR spectrum of (^{acri}PNP-Me)Ni–COMe (**5'**) in acetone-d_6 at room temperature.

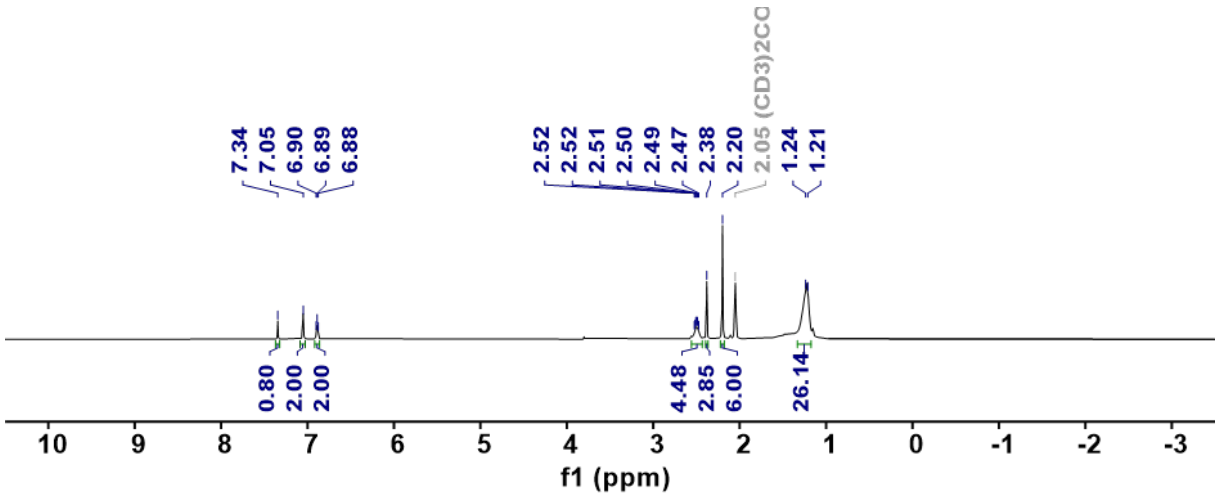

Figure S20. ^{13}C NMR spectrum of (^{acri}PNP-Me)Ni–COMe (**5'**) in C_6D_6 at room temperature.

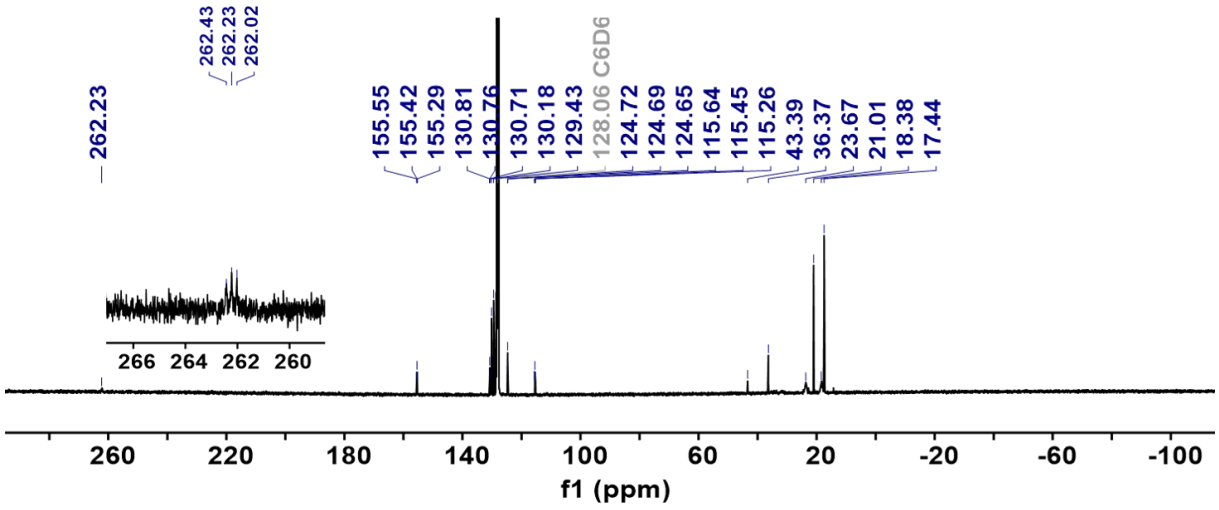

Figure S21. ^{31}P NMR spectrum of (^{acri}PNP-Me)Ni–COMe (**5'**) in C_6D_6 at room temperature.

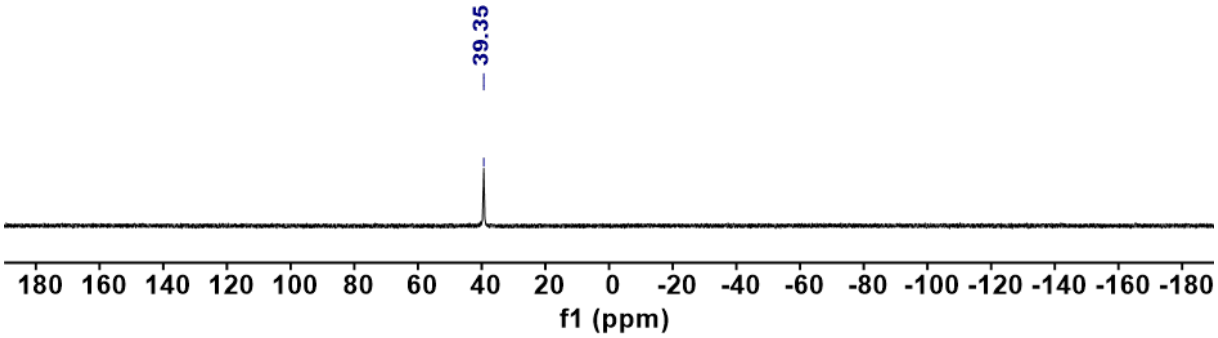

Figure S22. ^{31}P NMR spectra (in C_6D_6 at RT) of the reactions of (^{acri}PNP-Ph)Ni–CO (**2**) with MeI at – 35 °C. (● Ni–COMe, ● Ni–Me, ● Ni–I)

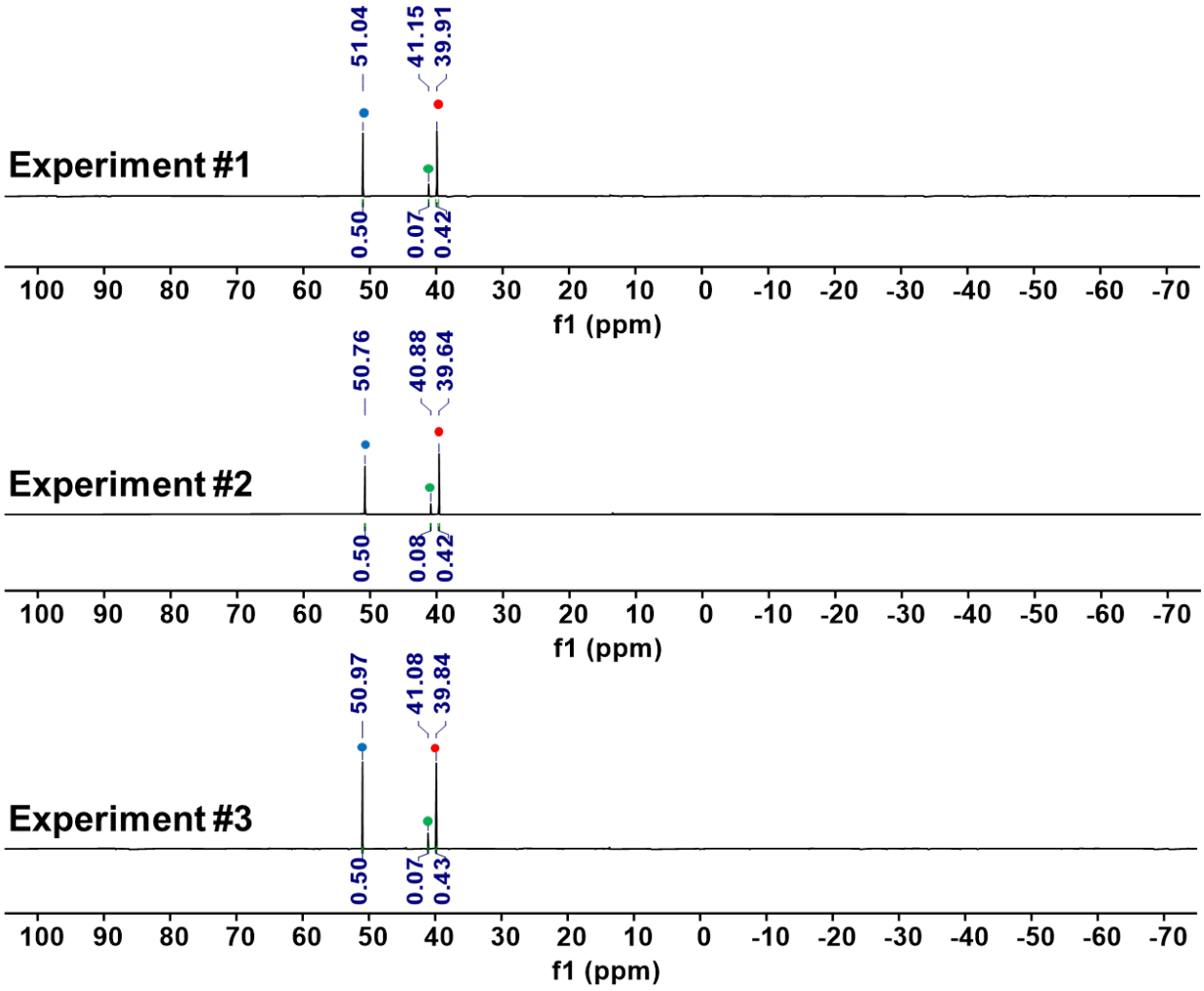

Figure S23. ^{31}P NMR spectra (in C_6D_6 at RT) of the reactions of (^{acri}PNP-Ph)Ni–CO (**2**) with MeI at RT. (● Ni–COMe, ● Ni–Me, ● Ni–I)

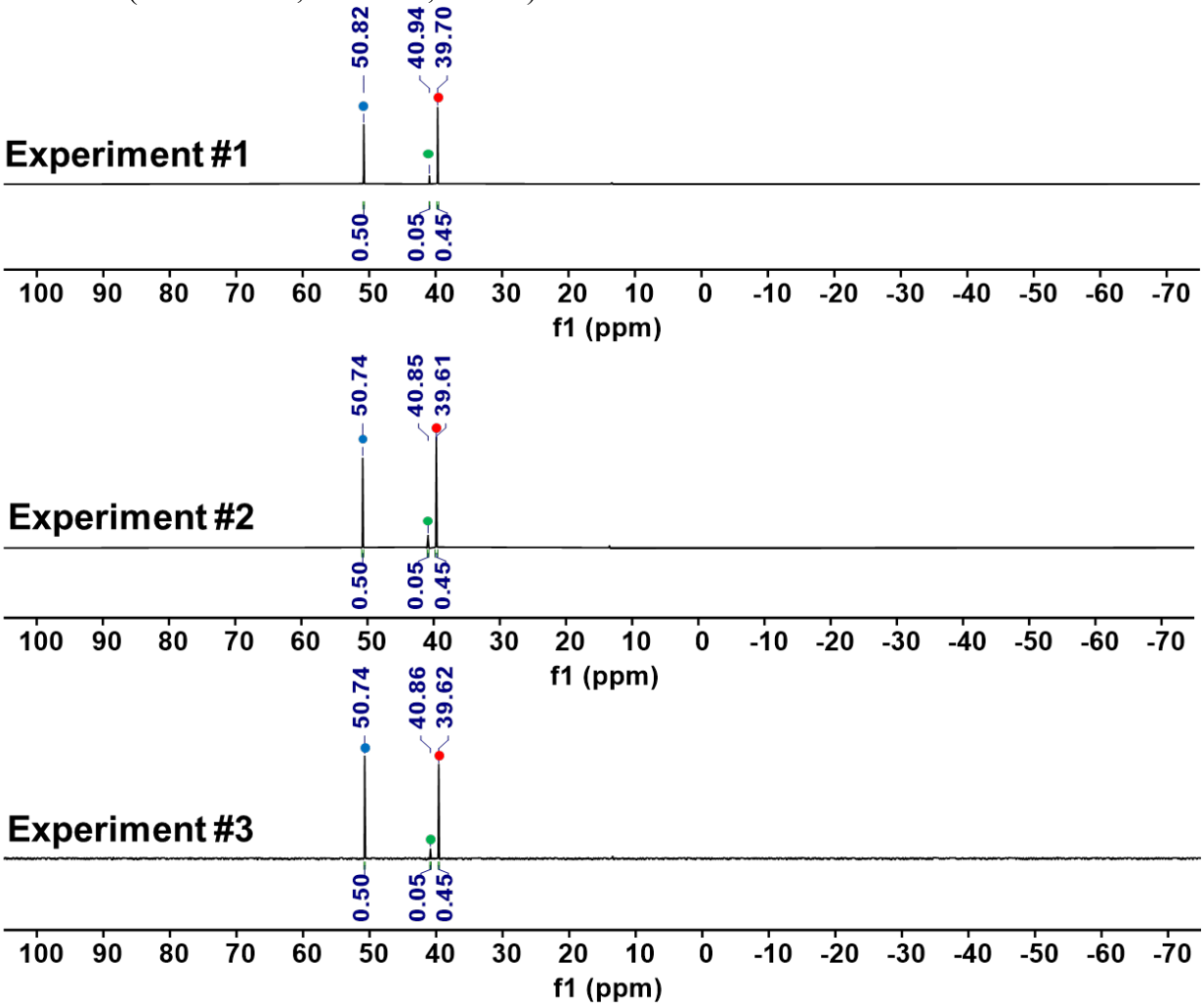

Figure S24. ^{31}P NMR spectra (in C_6D_6 at RT) of the reactions of (^{acri}PNP-Me)Ni–CO (**2'**) with MeI at – 35 °C. (● Ni–COMe, ● Ni–Me, ● Ni–I)

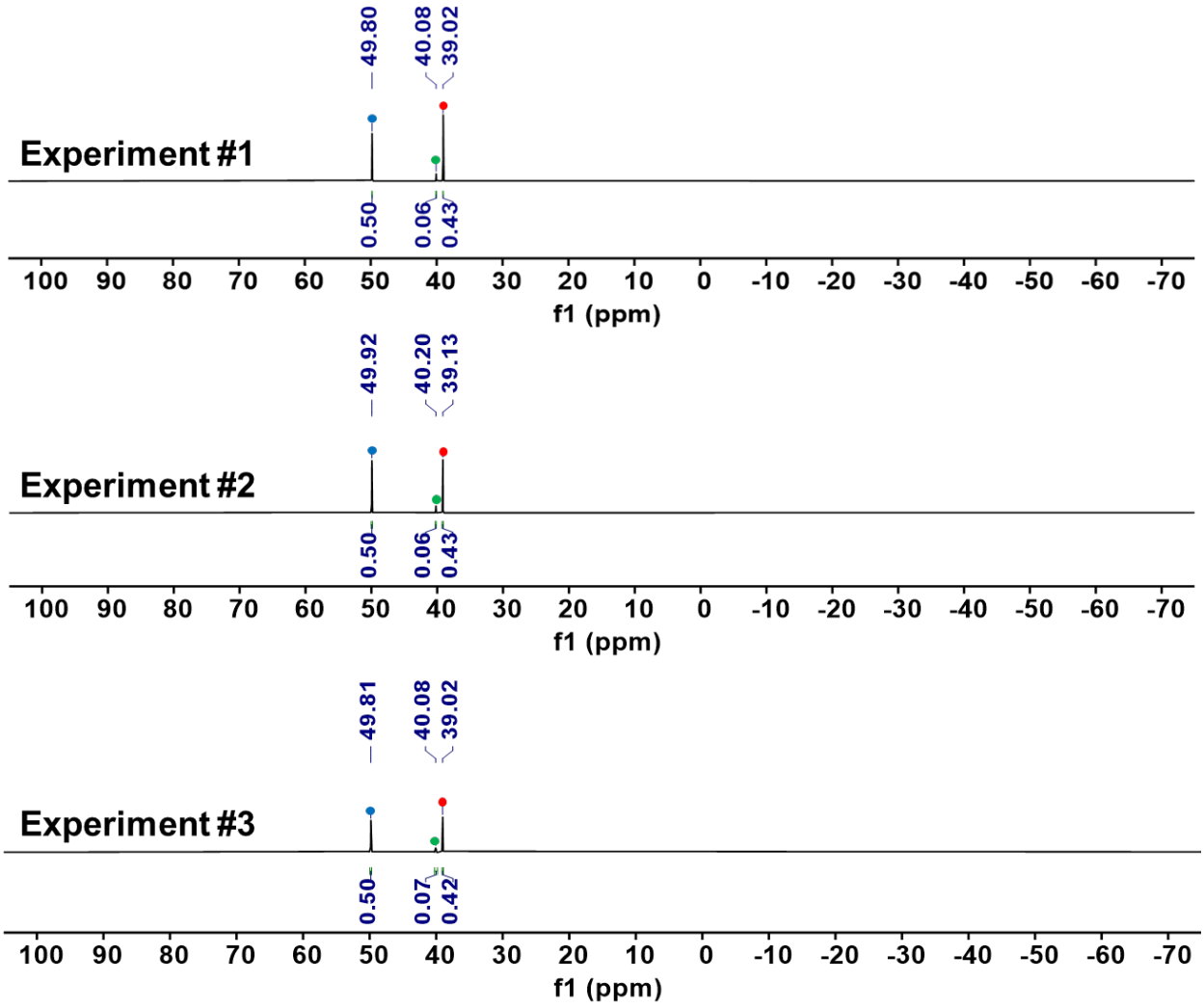

Figure S25. ^{31}P NMR spectra (in C_6D_6 at RT) of the reactions of (^{acri}PNP-Me)Ni–CO (**2'**) with MeI at RT. (● Ni–COMe, ● Ni–Me, ● Ni–I)

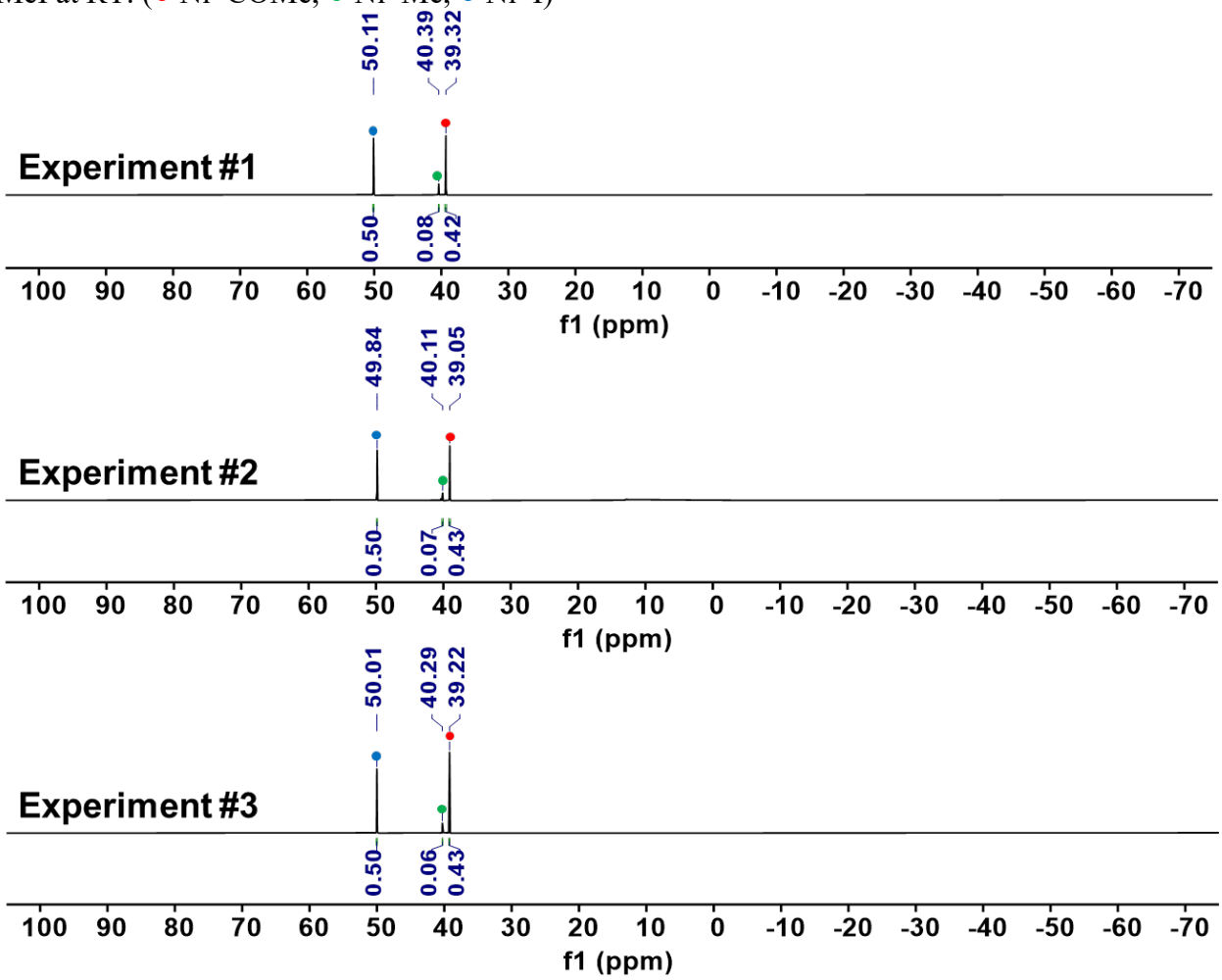

Figure S26. ^{31}P NMR spectra (in C_6D_6 at RT) of the reactions of {Na}{(^{acri}PNP-Ph)Ni–CO} (**3**) with MeI at – 35 °C. (● Ni–COMe, ● Ni–Me)

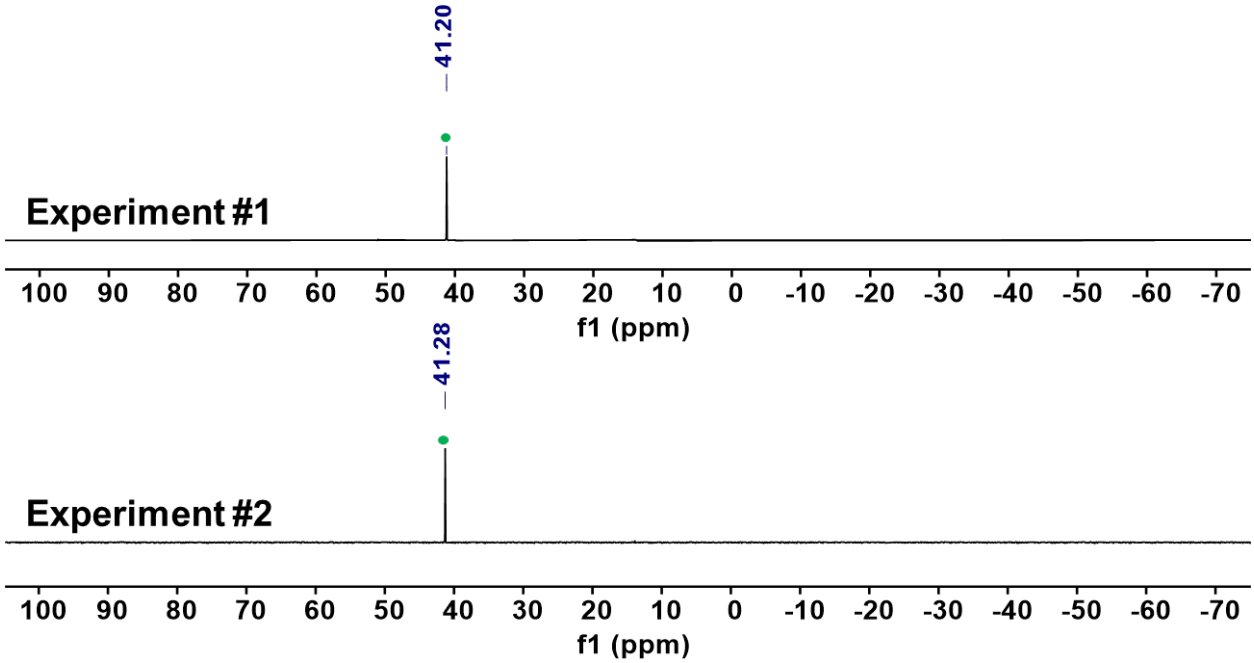

Figure S27. ^{31}P NMR spectra (in C_6D_6 at RT) of the reactions of {Na}{(^{acri}PNP-Ph)Ni–CO} (**3**) with MeI at RT. (● Ni–COMe, ● Ni–Me)

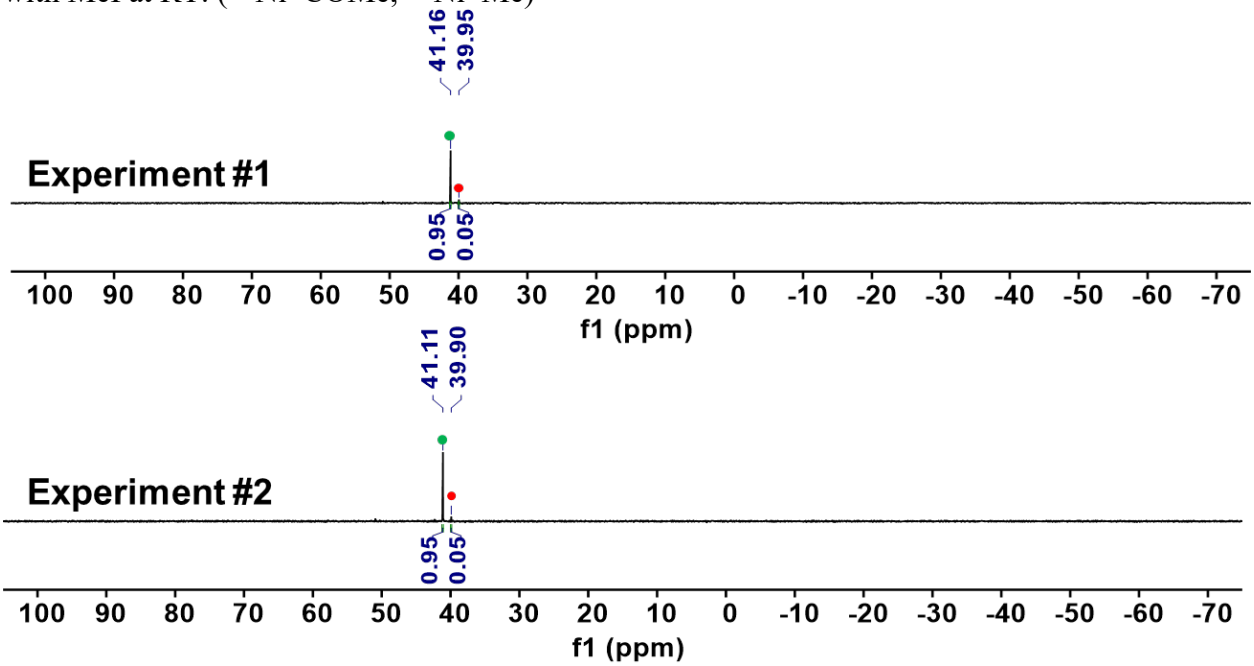

Figure S28. ^{31}P NMR spectra (in C_6D_6 at RT) of the reactions of {Na}{(^{acri}PNP-Me)Ni–CO} (**3'**) with MeI at – 35 °C. (● Ni–COMe, ● Ni–Me)

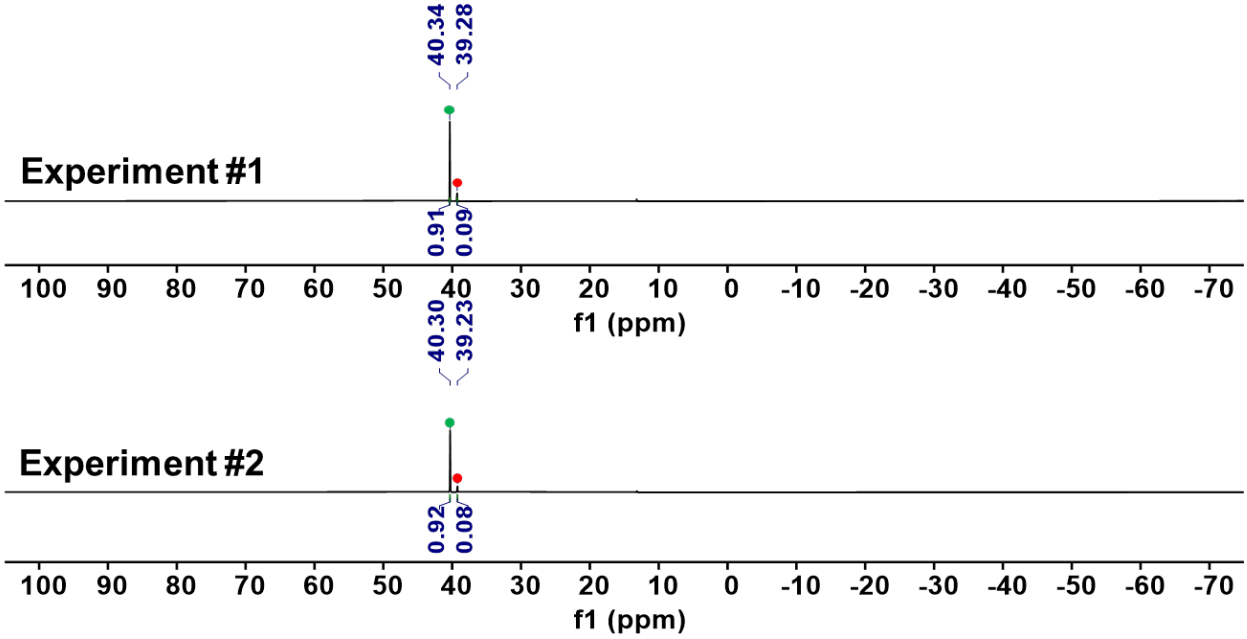

Figure S29. ^{31}P NMR spectra (in C_6D_6 at RT) of the reactions of {Na}{(^{acri}PNP-Me)Ni(CO)} (**3'**) with MeI at RT. (● Ni–COMe, ● Ni–Me)

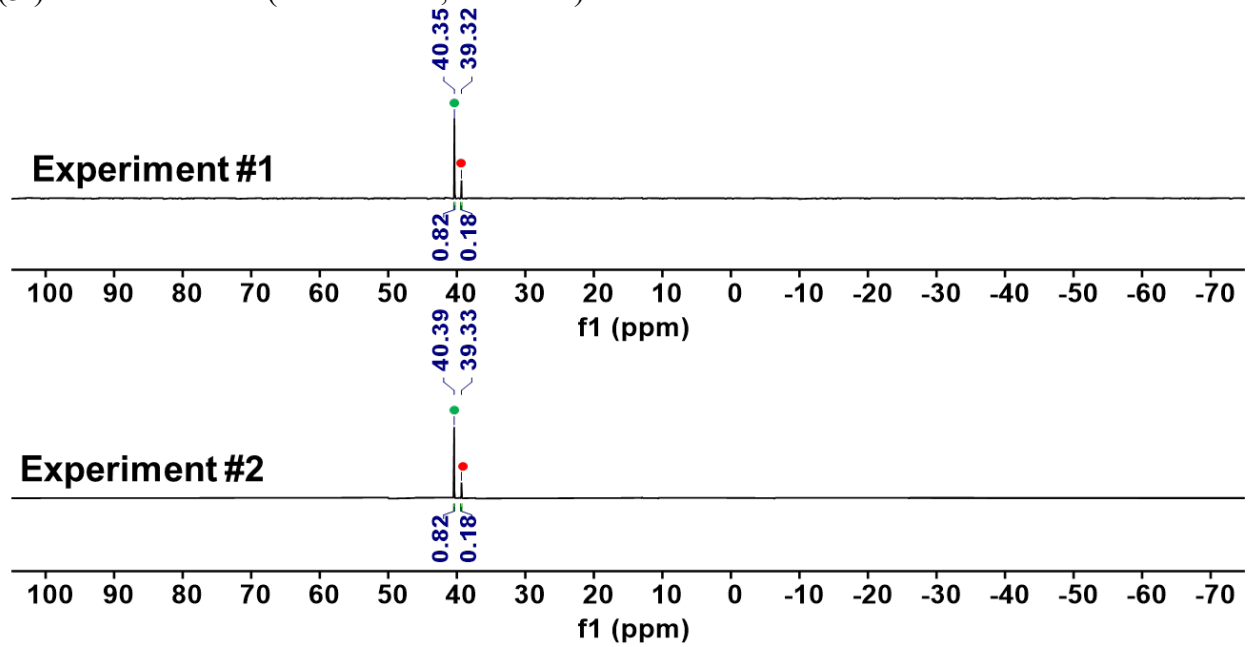

Figure S30. ^{31}P NMR spectra (in C_6D_6 at RT) of the reactions of {Na}{(^{acri}PNP-Ph)Ni–CO} (**3**) with EtI at – 35 °C. (▲Ni–COEt, ▲ Ni–Et)

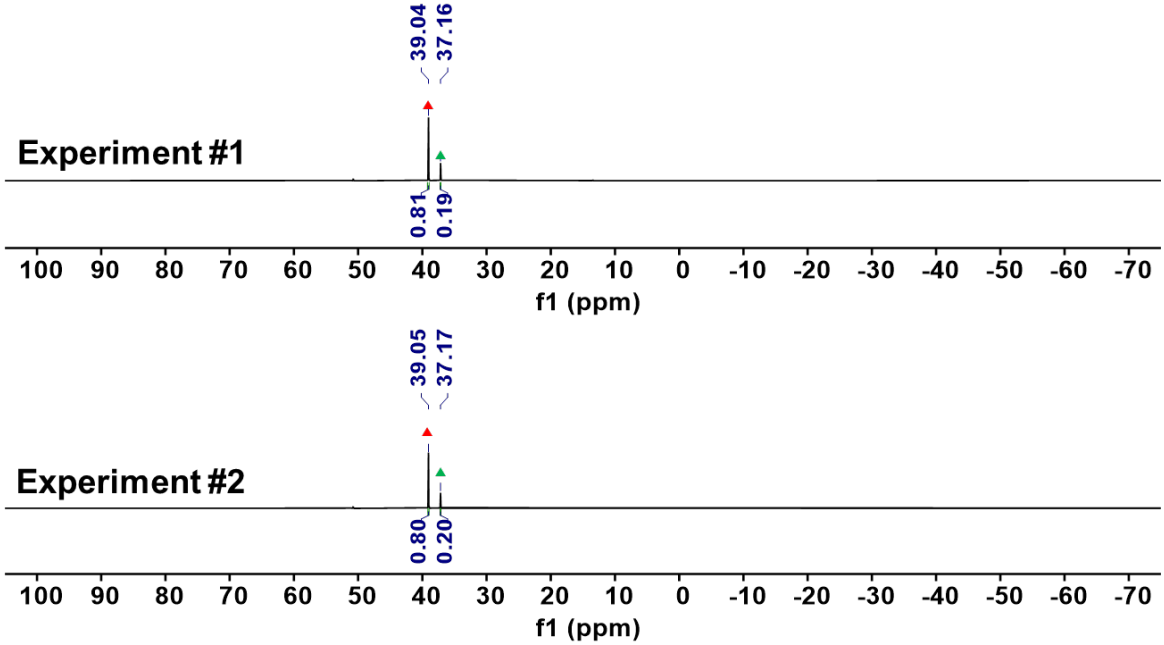

Figure S31. ^{31}P NMR spectra (in C_6D_6 at RT) of the reactions of {Na}{(^{acri}PNP-Ph)Ni–CO} (**3**) with EtI at RT. (▲Ni–COEt, ▲ Ni–Et)

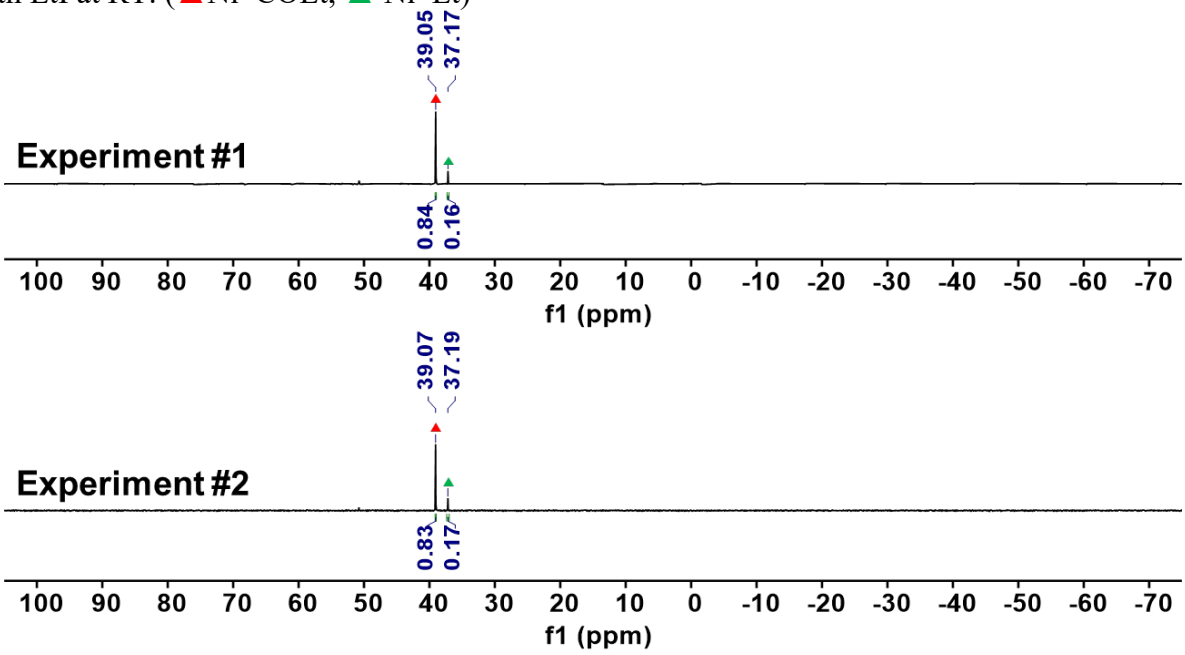

Figure S32. ^{31}P NMR spectra (in C_6D_6 at RT) of the reactions of {Na}{(^{acri}PNP-Me)Ni–CO} (**3'**) with EtI at – 35 °C. (▲Ni–COEt, ▲ Ni–Et)

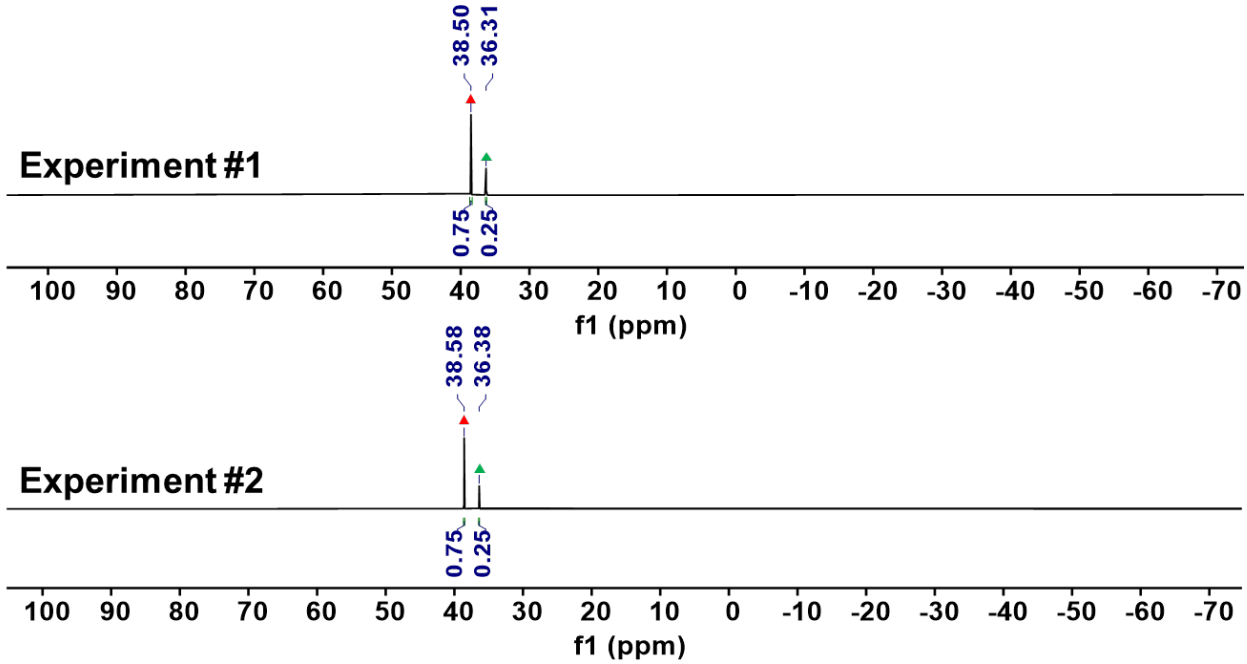

Figure S33. ^{31}P NMR spectra (in C_6D_6 at RT) of the reactions of {Na}{(^{acri}PNP-Me)Ni–CO} (**3'**) with EtI at RT. (▲Ni–COEt, ▲ Ni–Et)

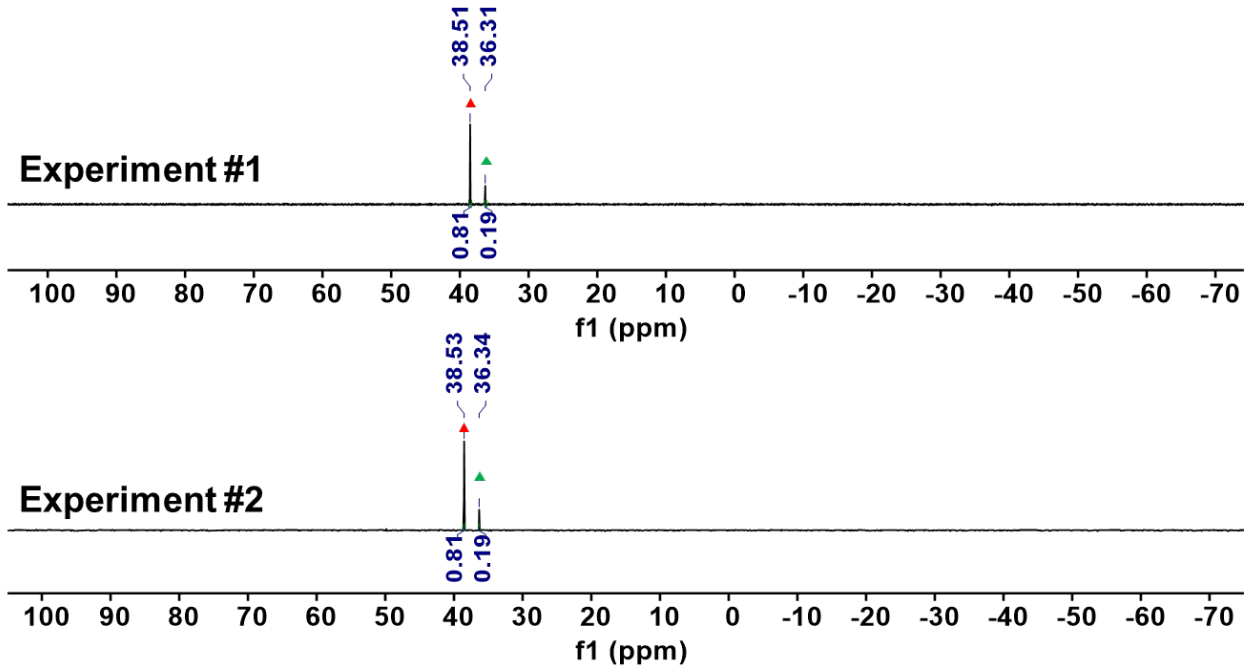

Figure S34. ^{31}P NMR spectra (in C_6D_6 at RT) of the reactions of {Na}{(^{acri}PNP-Ph)Ni–CO} (**3**) with ^{t}BuI at – 35 °C. (▲ Ni–I, ▲ Ni–CO^{t}Bu)

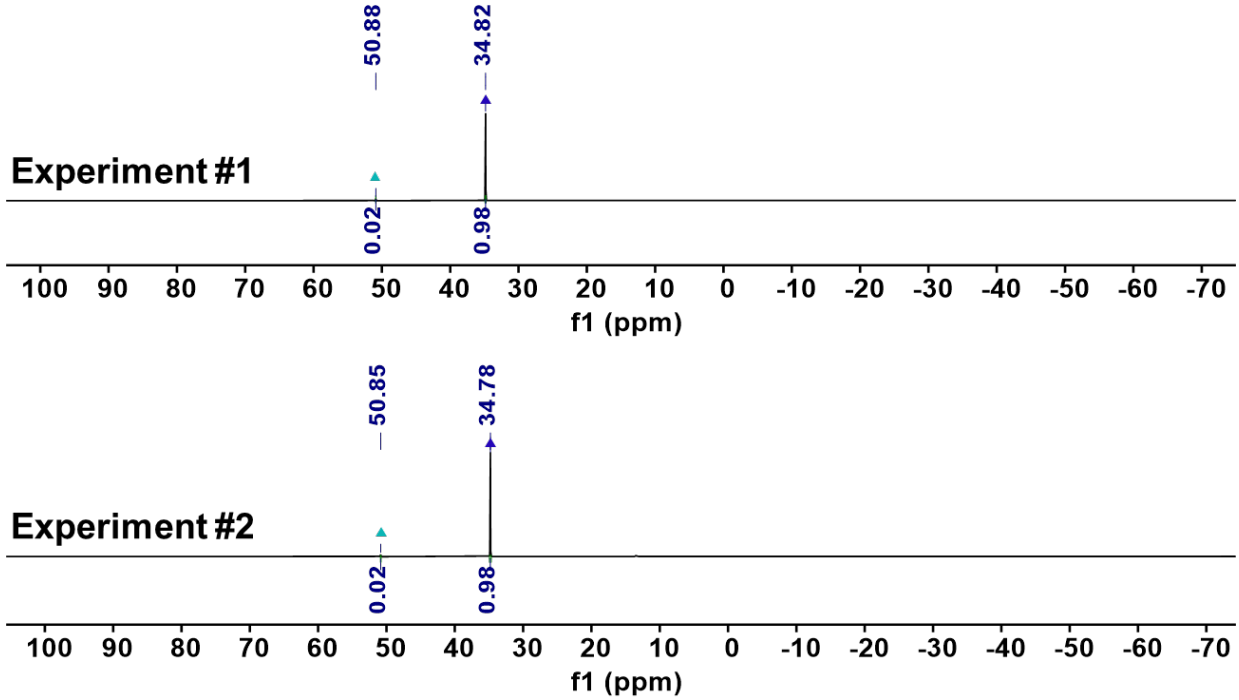

Figure S35. ^{31}P NMR spectra (in C_6D_6 at RT) of the reactions of {Na}{(^{acri}PNP-Me)Ni–CO} (**3'**) with ^{t}BuI at – 35 °C. (▲ Ni–I, ▲ Ni–CO^{t}Bu)

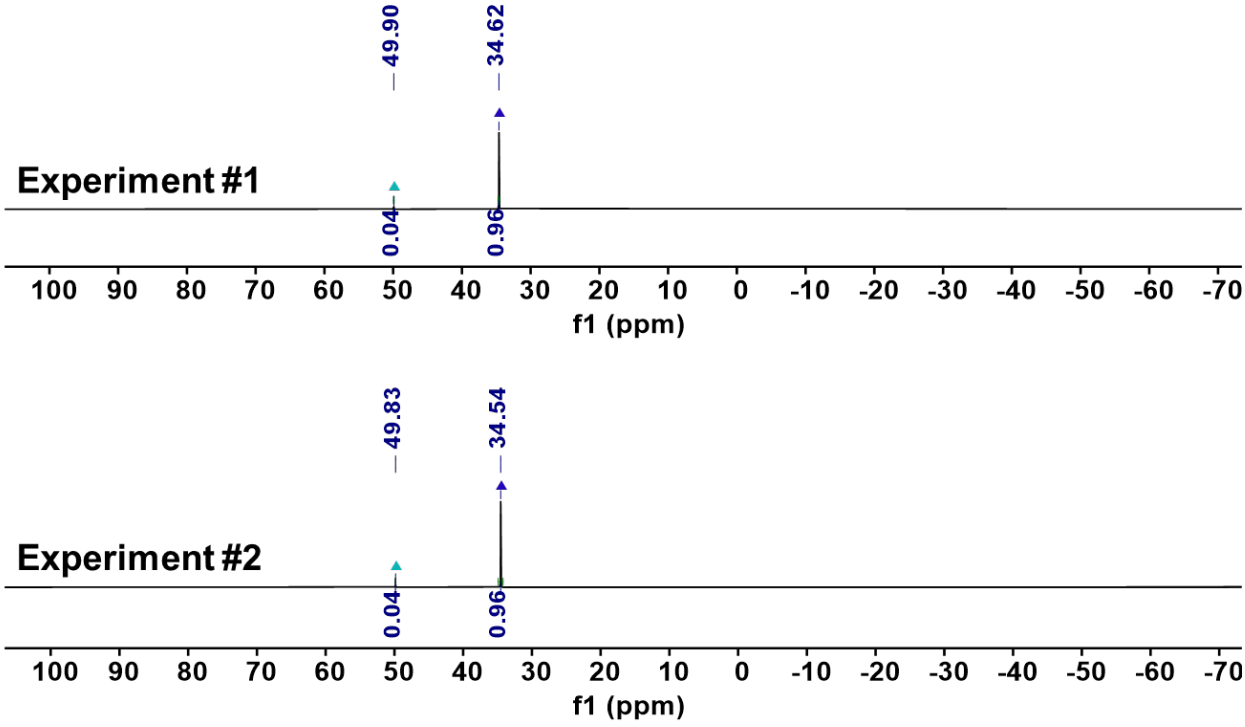

Figure S36. Experimental (black line) and simulated (dashed red line) X-Band EPR spectrum of (^{acri}PNP-Ph)Ni•$C_{10}H_8$ (**1**•$C_{10}H_8$) in toluene at 20K.

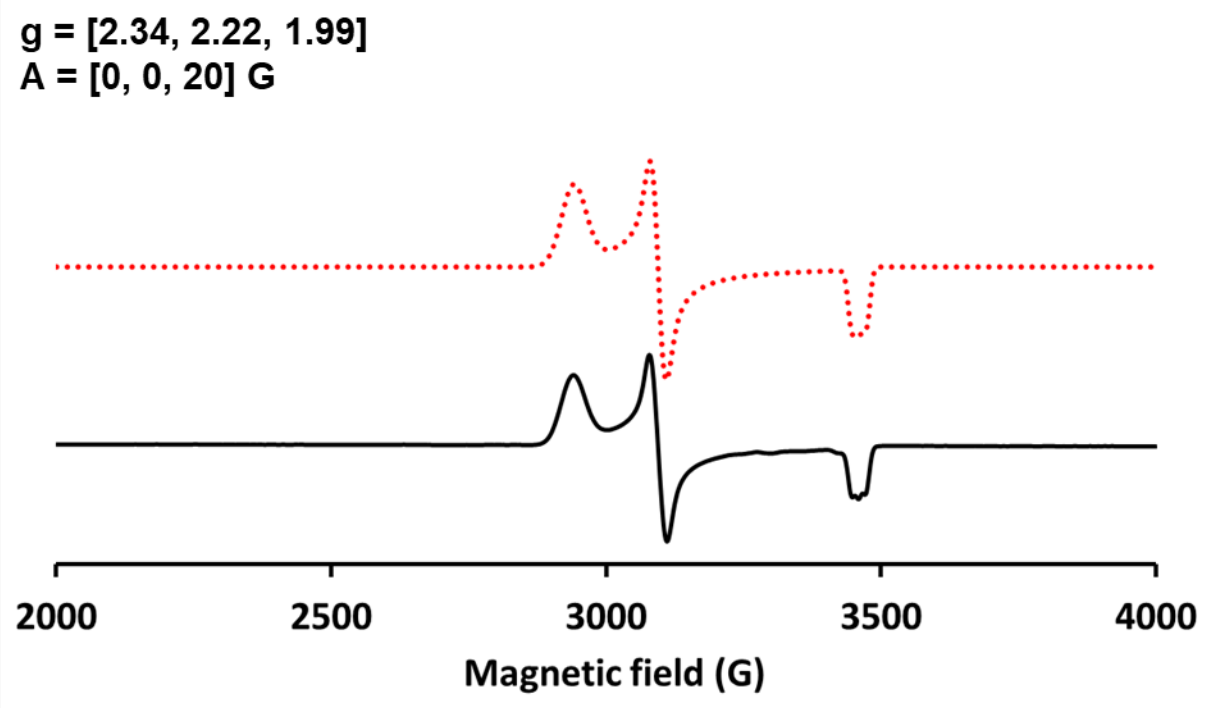

Figure S37. Experimental (black line) and simulated (dashed red line) X-Band EPR spectrum of (^{acri}PNP-Ph)Ni–CO (**2**) in toluene (black) at 20K.

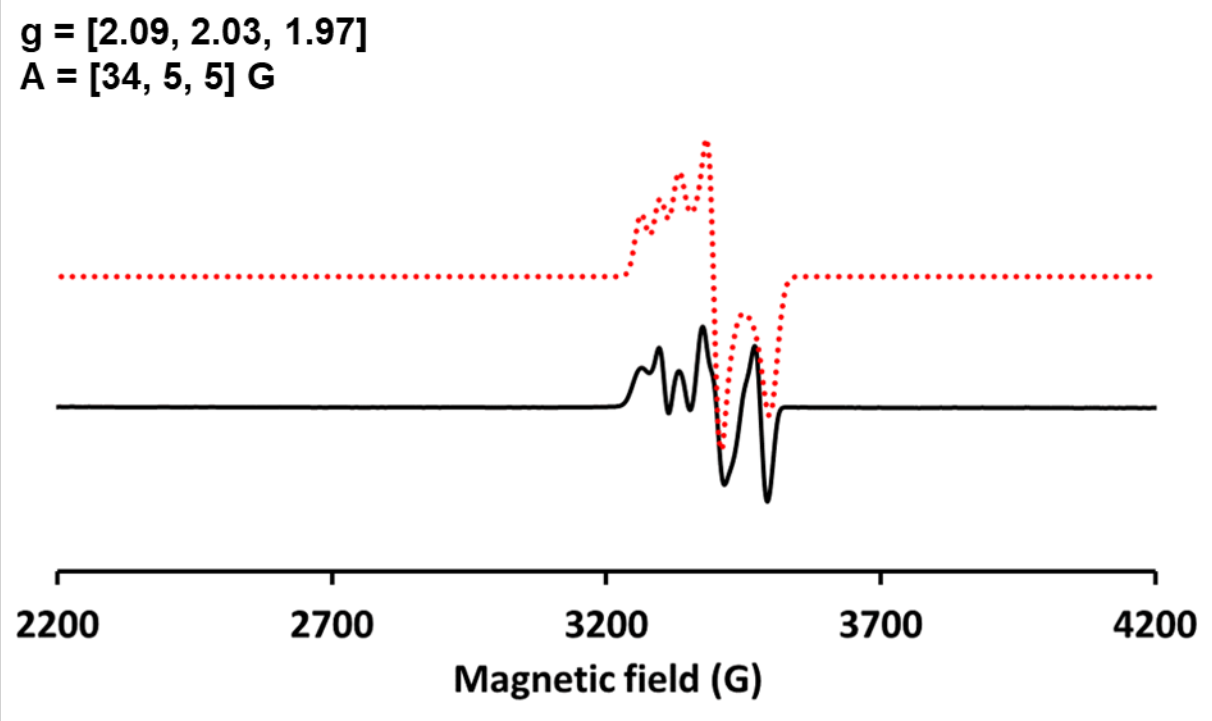

Figure S38. Solid-state structure of (^{acri}PNP-Ph)Ni–Br. Hydrogen atoms are omitted for clarity.

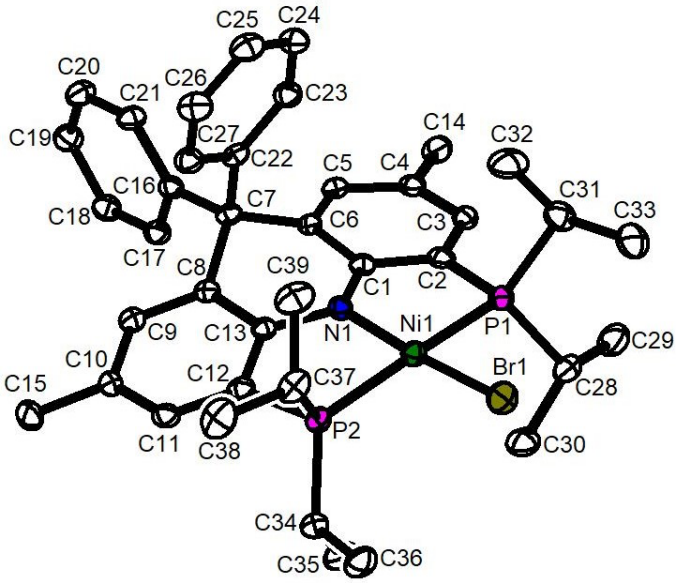

Table S1. Selected bond distances and angles of (^{acri}PNP-Ph)Ni–Br (Å and °).

Bond Distance		Bond Angle	
d_{Ni1-N1}	1.885(3)	∠N1-Ni1-Br1	173.24(8)
d_{Ni1-P1}	2.1923(9)	∠P1-Ni1-P2	167.90(4)
d_{Ni1-P2}	2.1973(9)	∠P1-Ni1-N1	86.50(8)
$d_{Ni1-Br1}$	2.3244(5)	∠P2-Ni1-N1	86.38(8)
		∠P1-Ni1-Br1	94.26(3)
		∠P2-Ni1-Br1	93.97(3)

Figure S39. Solid-state structure of (^{acri}PNP-Ph)Ni (**1**). Hydrogen atoms are omitted for clarity.

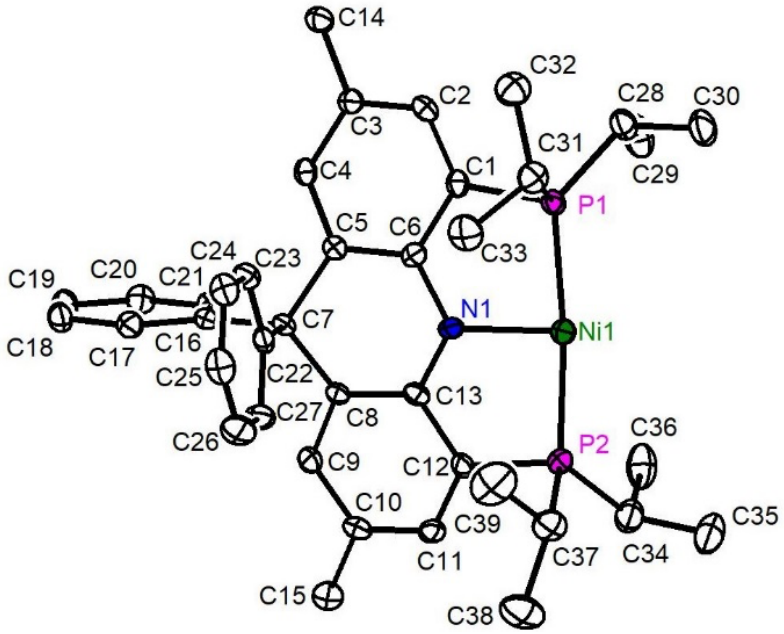

Table S2. Selected bond distances and angles of (^{acri}PNP-Ph)Ni (**1**) (Å and °).

Bond Distance		Bond Angle	
$d_{Ni1\text{-}N1}$	1.932(2)	∠P1-Ni1-P2	174.30 (3)
$d_{Ni1\text{-}P1}$	2.1897(9)	∠P1-Ni1-N1	87.06(8)
$d_{Ni1\text{-}P2}$	2.1932(9)	∠P2-Ni1-N1	87.36(8)

Figure S40. Solid-state structure of ([acri]PNP-Ph)Ni–CO (**2**). Hydrogen atoms are omitted for clarity.

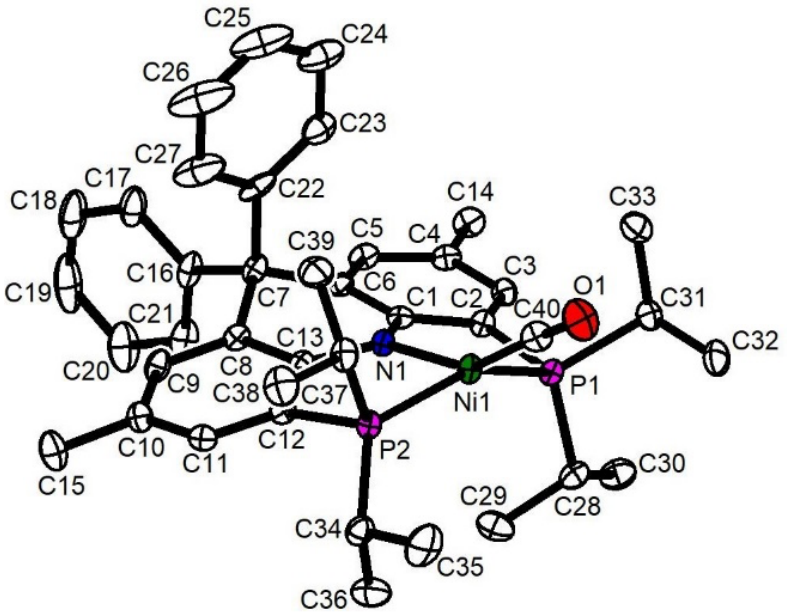

Table S3. Selected bond distances and angles of ([acri]PNP-Ph)Ni–CO (**2**) (Å and °).

Bond Distance		Bond Angle	
$d_{Ni1\text{-}N1}$	1.936(2)	∠P1-Ni1-P2	150.09(3)
$d_{Ni1\text{-}P1}$	2.2481(7)	∠N1-Ni1-C40	148.49(1)
$d_{Ni1\text{-}P2}$	2.2525(7)	∠Ni1-C40-O1	176.3(3)
$d_{Ni1\text{-}C40}$	1.775(3)	∠P1-Ni1-N1	84.83(6)
$d_{C40\text{-}O1}$	1.145(3)	∠P2-Ni1-N1	85.36(3)
		∠P1-Ni1-C40	103.81(9)
		∠P2-Ni1-C40	99.27(9)

Figure S41. Solid-state structure of {Na(12-C-4)$_2$}{(^{acri}PNP-Ph)Ni(CO)} (**3** · (12-C-4)$_2$). Hydrogen atoms are omitted for clarity.

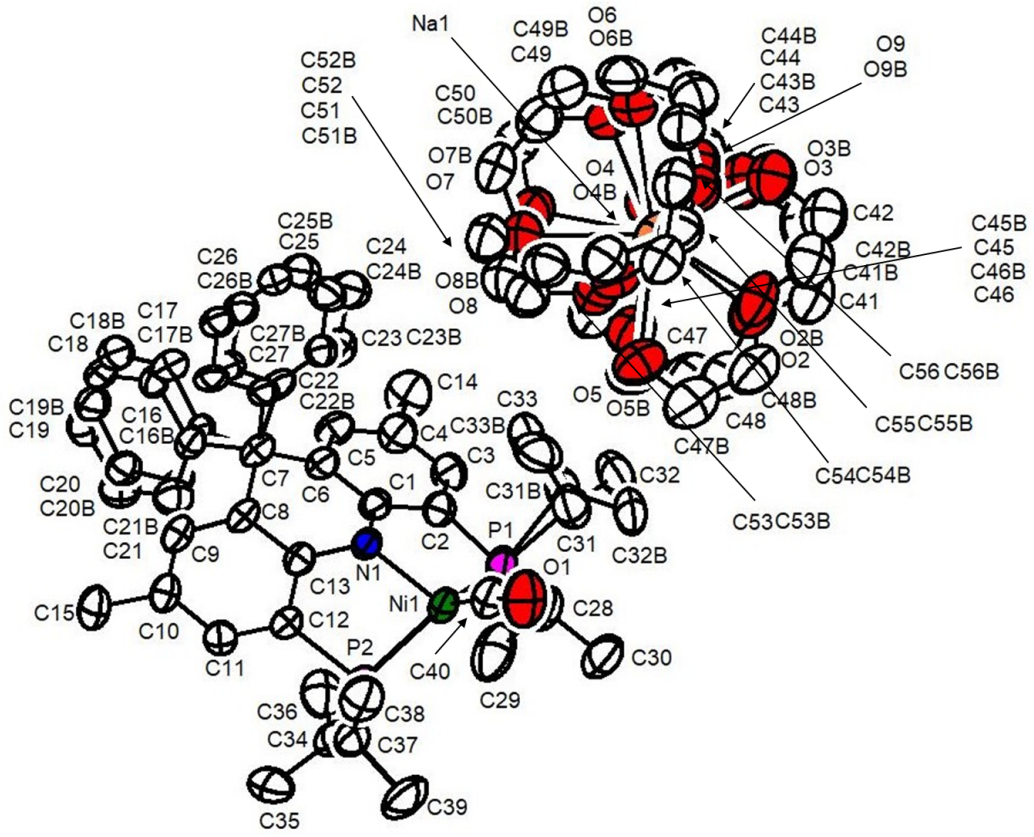

Table S4. Selected bond distances and angles of {Na(12-C-4)$_2$}{(^{acri}PNP-Ph)Ni(CO)} (**3**·(12-C-4)$_2$) (Å and °).

Bond Distance		Bond Angle	
$d_{Ni1\text{-}N1}$	2.029(3)	∠P1-Ni1-P2	133.36(5)
$d_{Ni1\text{-}P1}$	2.182(1)	∠N1-Ni1-C40	128.52(2)
$d_{Ni1\text{-}P2}$	2.186(1)	∠Ni1-C40-O1	172.5(4)
$d_{Ni1\text{-}C40}$	1.726(5)	∠P1-Ni1-N1	85.00(9)
$d_{C40\text{-}O1}$	1.173(6)	∠P2-Ni1-N1	83.59(9)
		∠P1-Ni1-C40	110.44(15)
		∠P2-Ni1-C40	111.98(15)

Figure S42. UV-Vis spectra of (^{acri}PNP-Ph)Ni(Br) (blue line), (^{acri}PNP-Ph)Ni•$C_{10}H_8$ (**1**, red line), (^{acri}PNP-Ph)Ni–CO (**2**, green line) {Na}{(^{acri}PNP-Ph)Ni–CO} (**3**, orange line) in THF at room temperature.

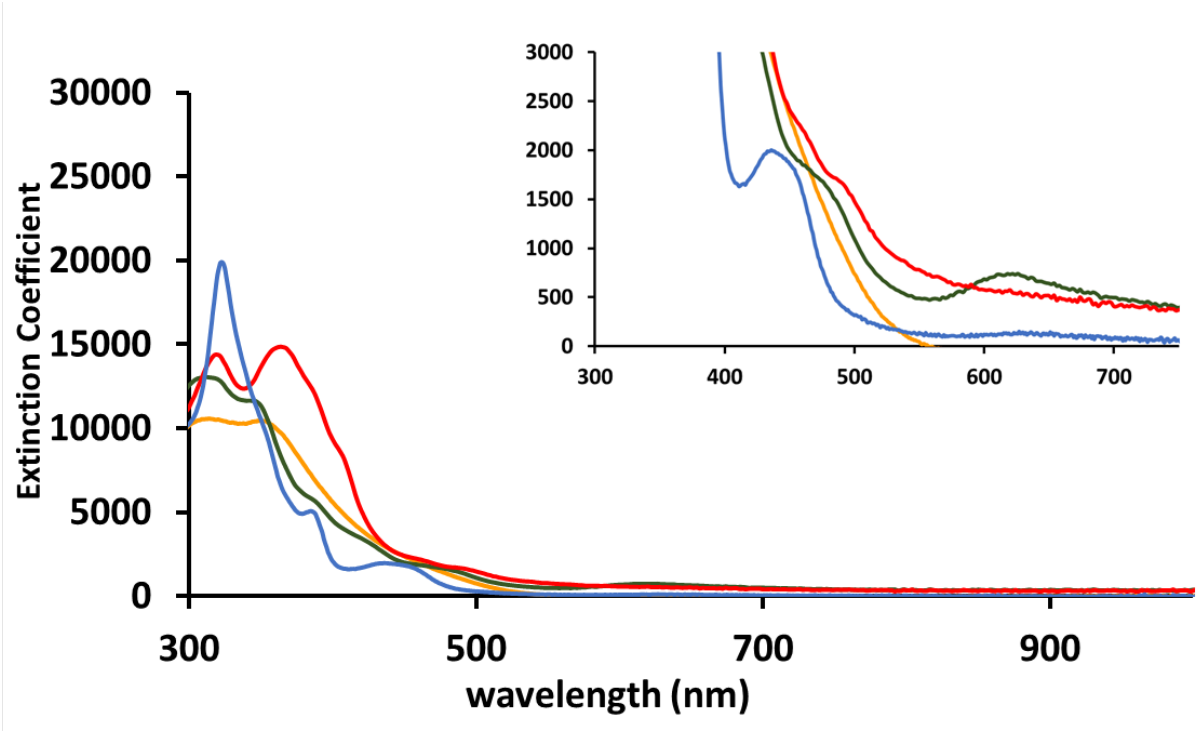

Figure S43. Cyclic voltammogram of (^{acri}PNP-Ph)Ni–CO (**2**) with scan rate: 100, 200, 300 and 400 mV/s. $Ni^{II/I}$ couple at –1.25 V and $Ni^{I/0}$ couple at –1.90 V vs. Fc/Fc^+ were observed in THF with 0.3 M tetra-n-butylammonium hexafluorophosphate as an electrolyte.

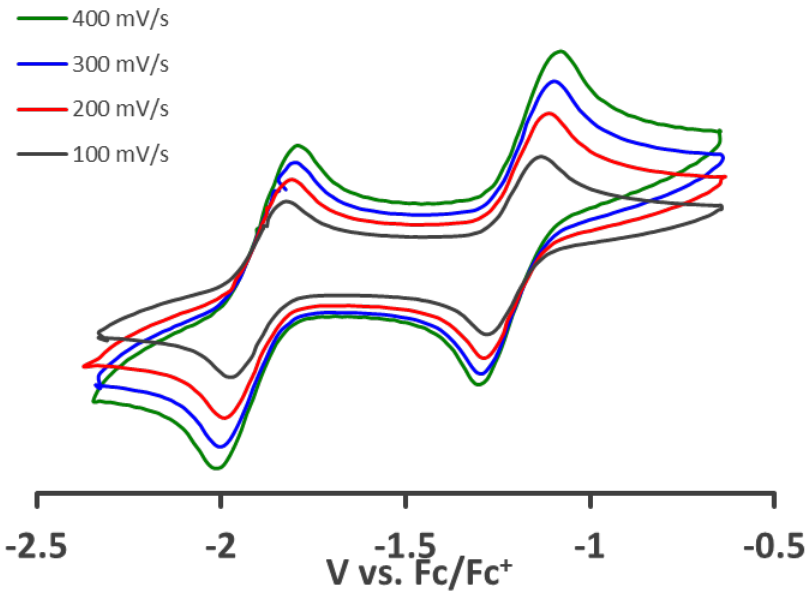

Figure S44. IR spectra of of (^{acri}PNP-Ph)Ni–Br (orange), (^{acri}PNP-Ph)Ni•$C_{10}H_8$ (**1**, blue), (^{acri}PNP-Ph)Ni–CO (**2**, green), {Na}{(^{acri}PNP-Ph)Ni–CO} (**3**, red) (KBr pellet).

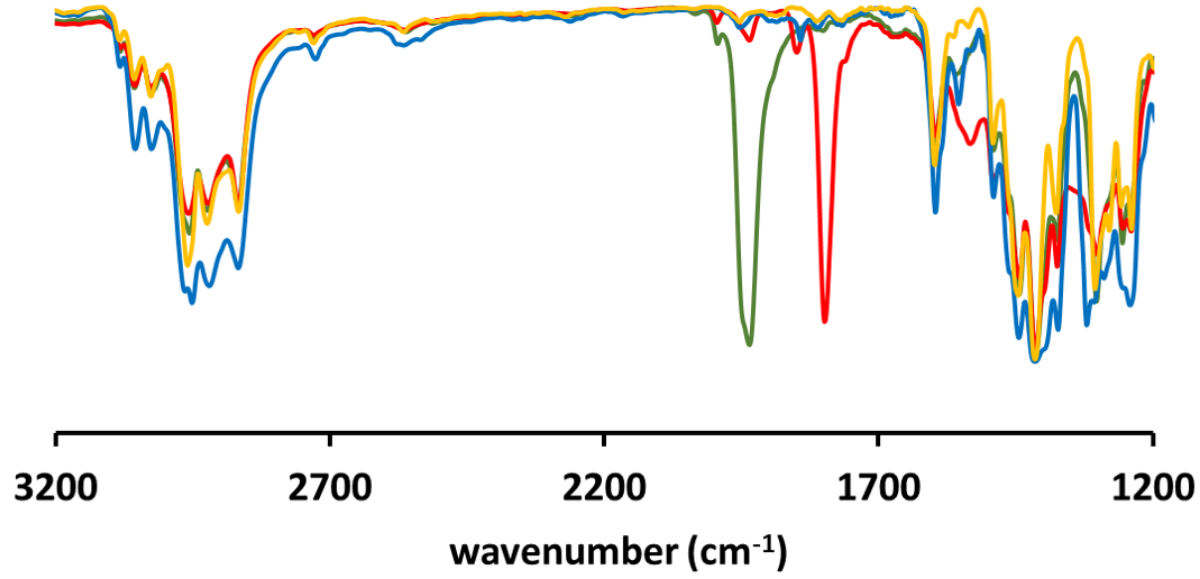

Figure S45. IR spectrum of of (^{acri}PNP-Ph)Ni–COMe (**5**) (KBr pellet).

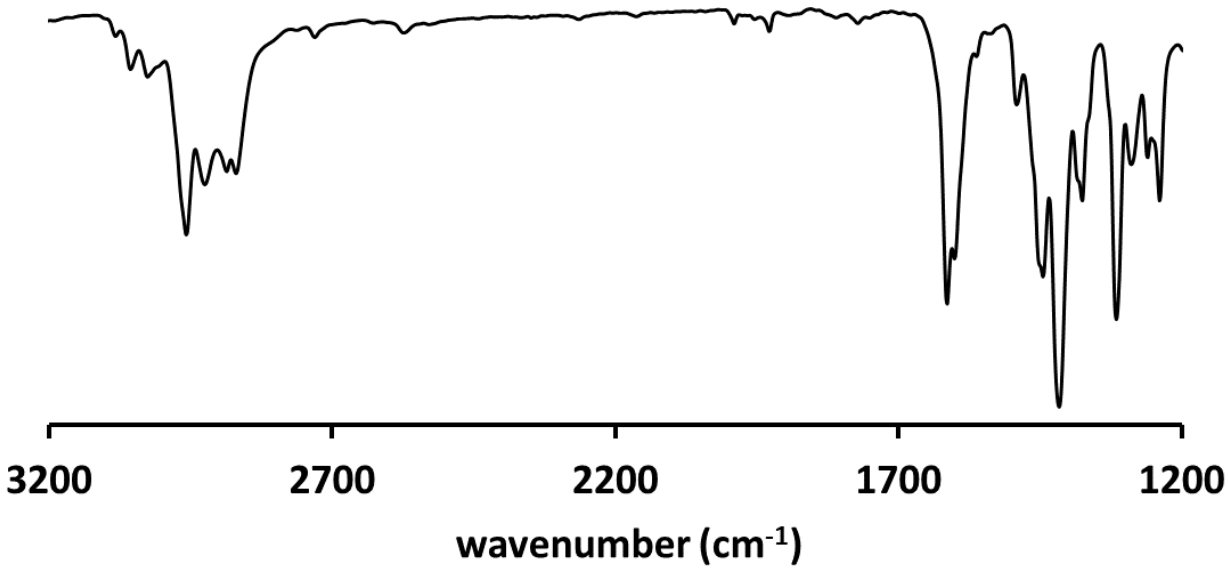

Figure S46. IR spectrum of of (^{acri}PNP-Me)Ni–COMe (**5'**) (KBr pellet).

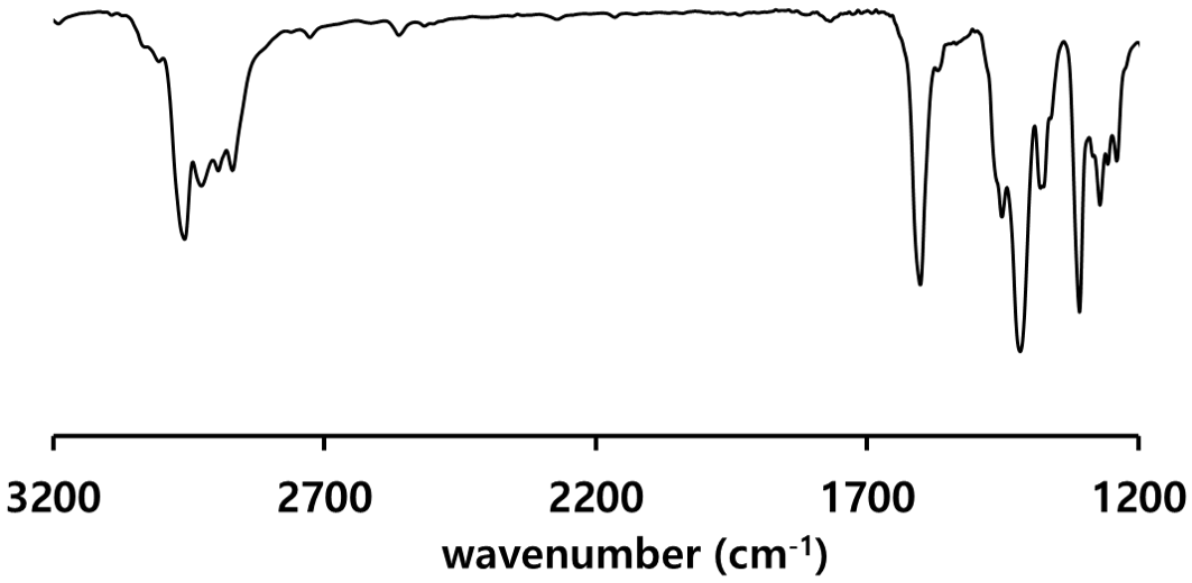

Figure S47. Space filling models of (a) anionic portion of {Na(12-C-4)$_2$}{(PNP)Ni–CO},[14] (b) **3**•(12-C-4)$_2$ and (c) **3'**•(12-C-4)$_2$.[2] Color code: green, Ni; blue, N; red, O; pink, P; gray, C; white, H.

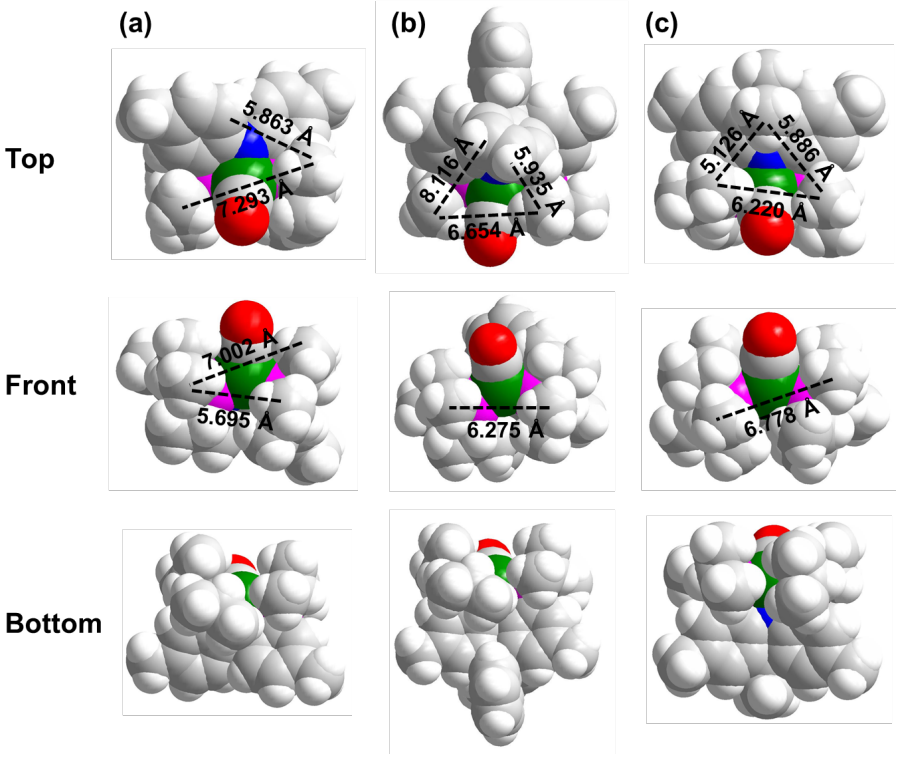

Figure S48. Buried volumes (V_{bur}) and *G*-parameters of (PNP)Ni–CO (a), **2** (b) and **2'** (c). Buried volume calculations were performed using the SambVca 2.1A web application with the use of a 5 Å sphere.[11,13] *G*-parameter calculations were performed using the Solid-G software.[12,13] The starting geometries were obtained from the X-ray crystallographic data.

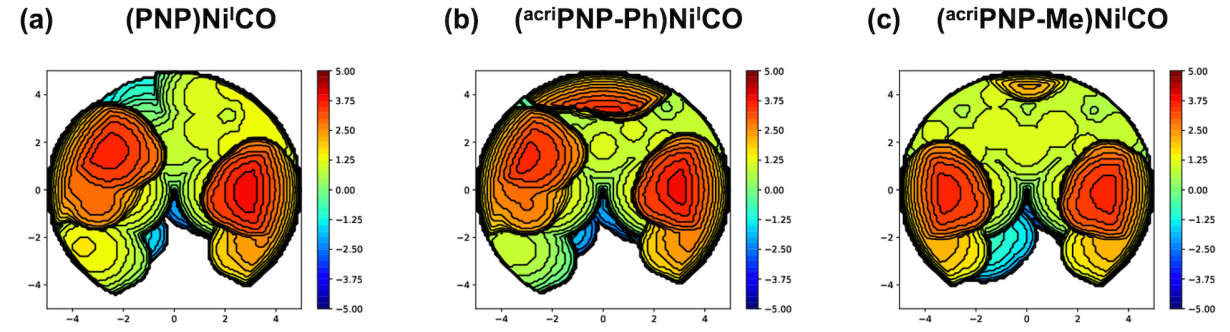

	(a)	(b)	(c)
V_{bur}	61.7%	62.5%	60.8%
G	65.9%	66.2%	65.5%

Figure S49. Buried volumes (V_{bur}) and *G*-parameters of anionic portions of [Na][(PNP)Ni–CO] (a), **3** (b) and **3'** (c). Buried volume calculations were performed using the SambVca 2.1A web application with the use of a 5 Å sphere.[11,13] *G*-parameter calculations were performed using the Solid-G software.[12,13] The starting geometries were obtained from the X-ray crystallographic data.

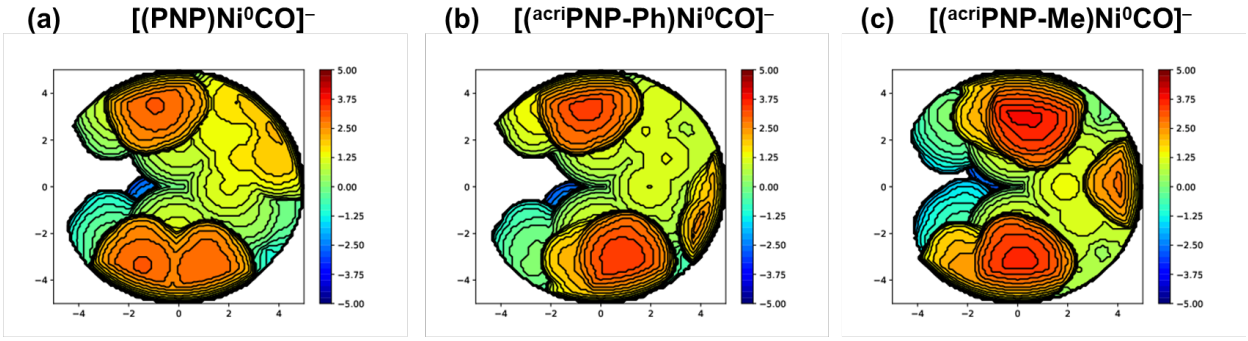

	(a)	(b)	(c)
V_{bur}	62.0%	61.0%	63.5%
G	65.0%	64.5%	66.9%

Figure S50. ESI-MS spectrum obtained in the solution of **4** (0.35 mM) under N_2 atmosphere in THF; the peak at m/z = 665.27 correspond to $[(^{acri}PNP\text{-}Ph)Ni–Me]^+$ (calcd. m/z 665.29). Black bars represent experiment values and red bars represent calculated values.

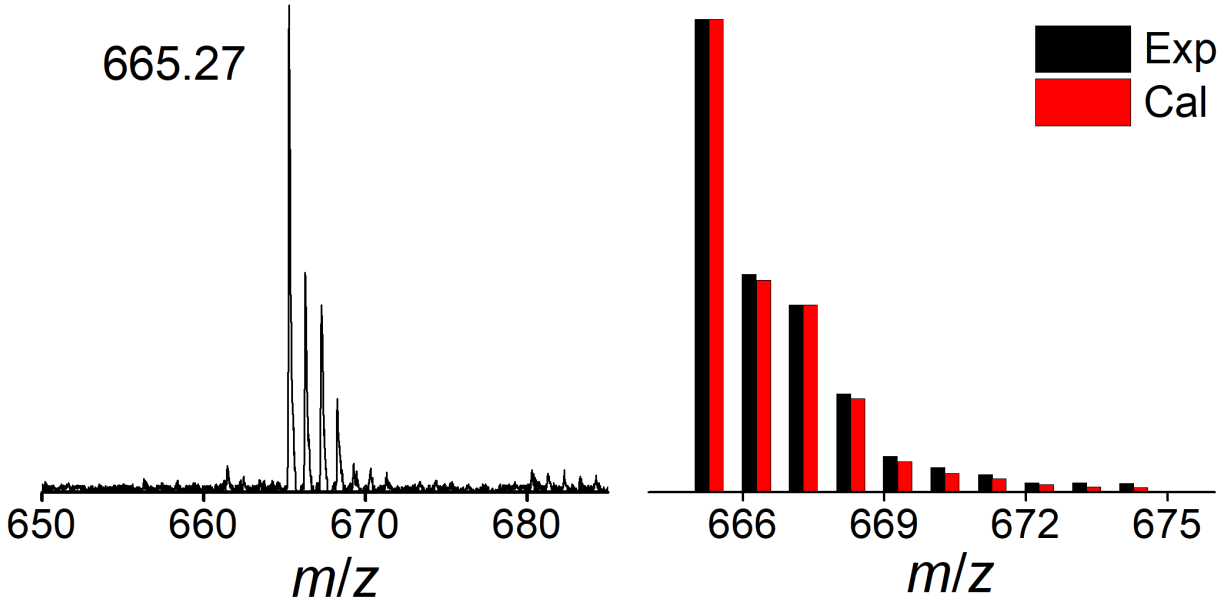

Figure S51. ESI-MS spectrum obtained in the solution of **5'** (0.35 mM) under N_2 atmosphere in THF; the peak at m/z = 569.25 correspond to $[(^{acri}PNP\text{-}Me)Ni–COMe]^+$ (calcd. m/z 569.25). Black bars represent experiment values and red bars represent calculated values. The peak at m/z = 567.24 represents acetonitrile bound species (minor impurity, blue bars are calculated values) resulting from washing process before the measurement.

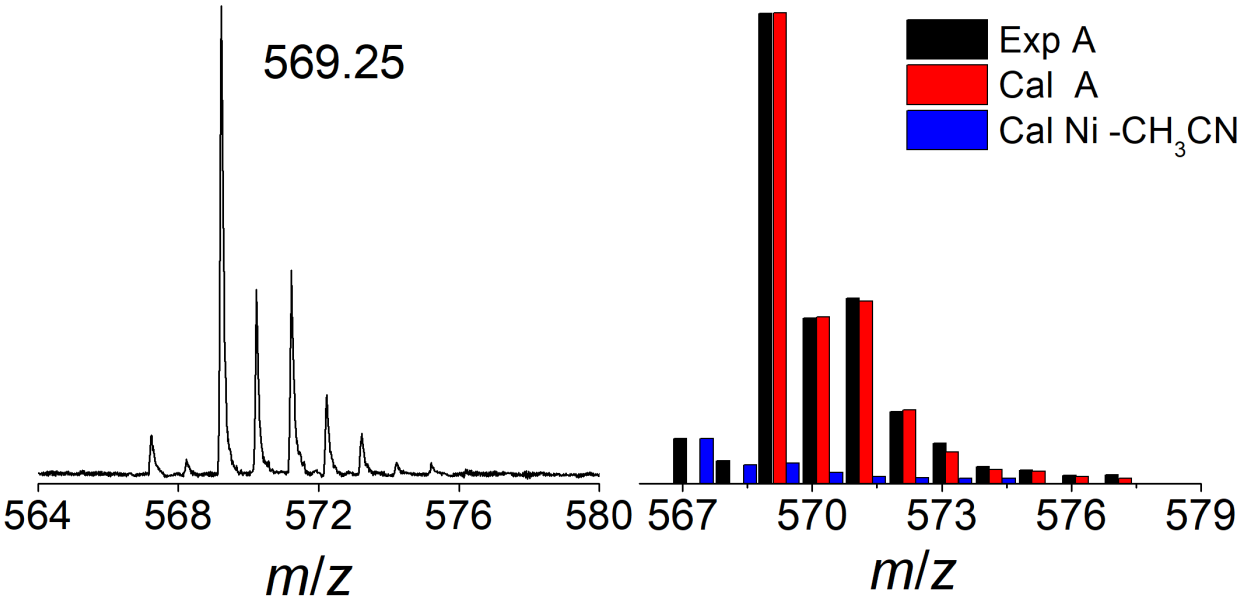

Figure S52. ESI-MS spectrum obtained from the solution of a reaction of **3** and EtI under N_2 atmosphere in THF**;** the peak at m/z = 708.33 correspond to $[(^{acri}PNP\text{-}Ph)Ni–COEt + H]^+$ (calcd. m/z 708.30) and the peak at m/z = 680.33 correspond to $[(^{acri}PNP\text{-}Ph)Ni–Et]^+$ (calcd. m/z 680.31).

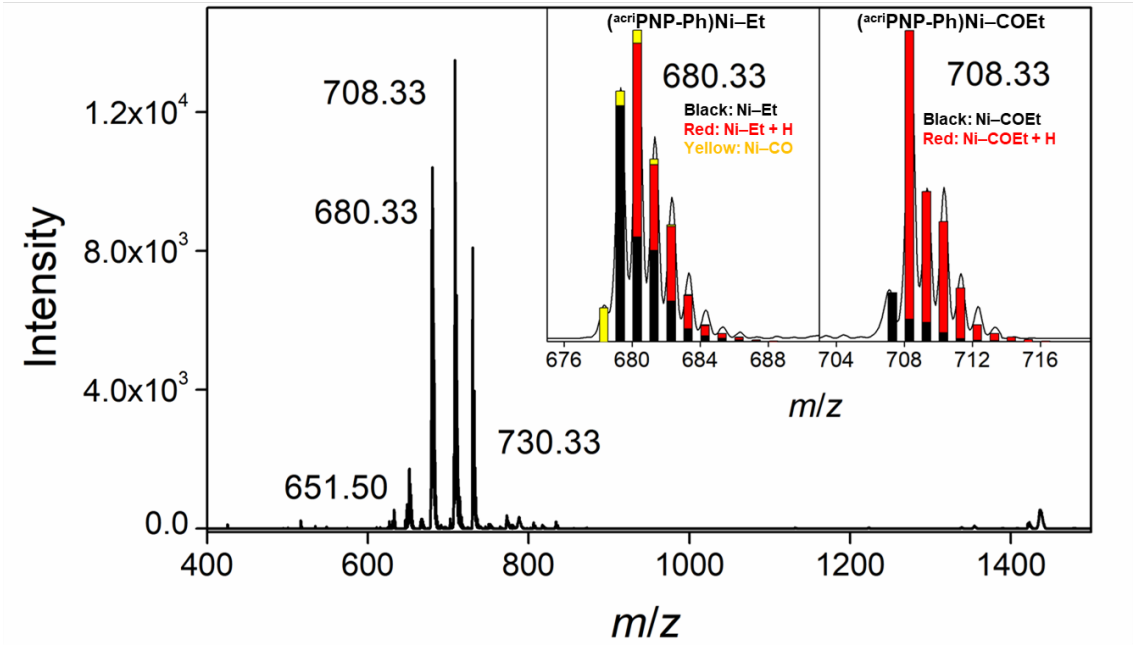

Figure S53. ESI-MS spectrum obtained from the solution of a reaction of **3** and ^{t}BuI under N_2 atmosphere in THF**;** the peak at m/z = 736.33 correspond to $[(^{acri}PNP\text{-}Ph)Ni–CO^tBu + H]^+$ (calcd. m/z 736.33) and the peak at m/z = 758.33 correspond to $[(^{acri}PNP\text{-}Ph)Ni– CO^tBu + Na]^+$ (calcd. m/z 758.32).

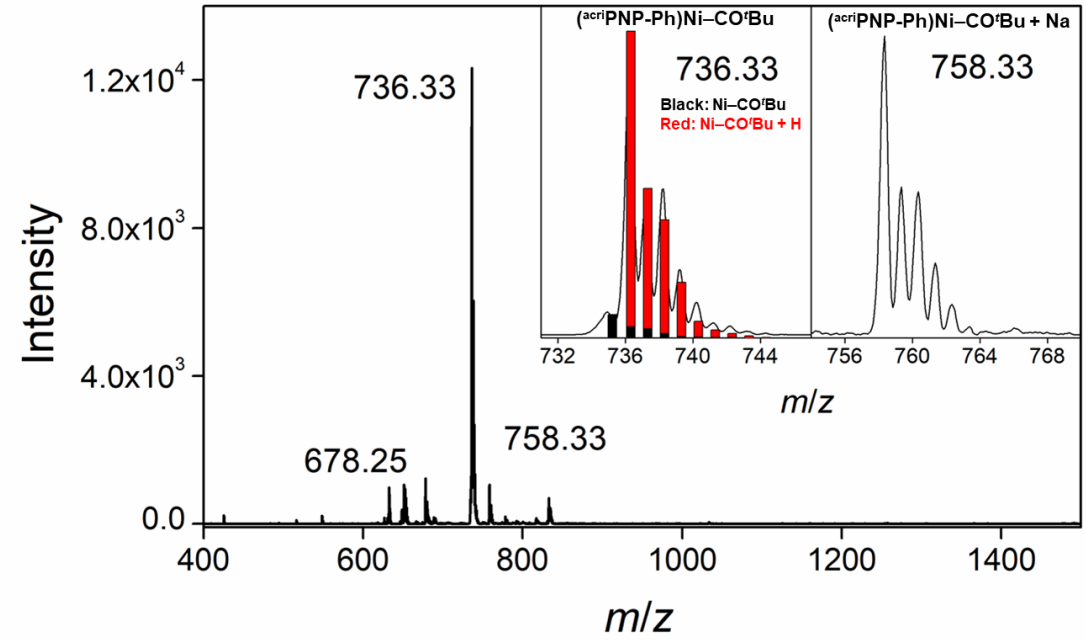

Figure S54. ESI-MS spectrum obtained from the solution of a reaction of **3'** and EtI under N_2 atmosphere in THF**;** the peak at m/z = 584.33 correspond to $[(^{acri}PNP\text{-}Me)Ni–COEt + H]^+$ (calcd. m/z 584.27) and the peak at m/z = 555.33 correspond to $[(^{acri}PNP\text{-}Me)Ni–Et]^+$ (calcd. m/z 555.27).

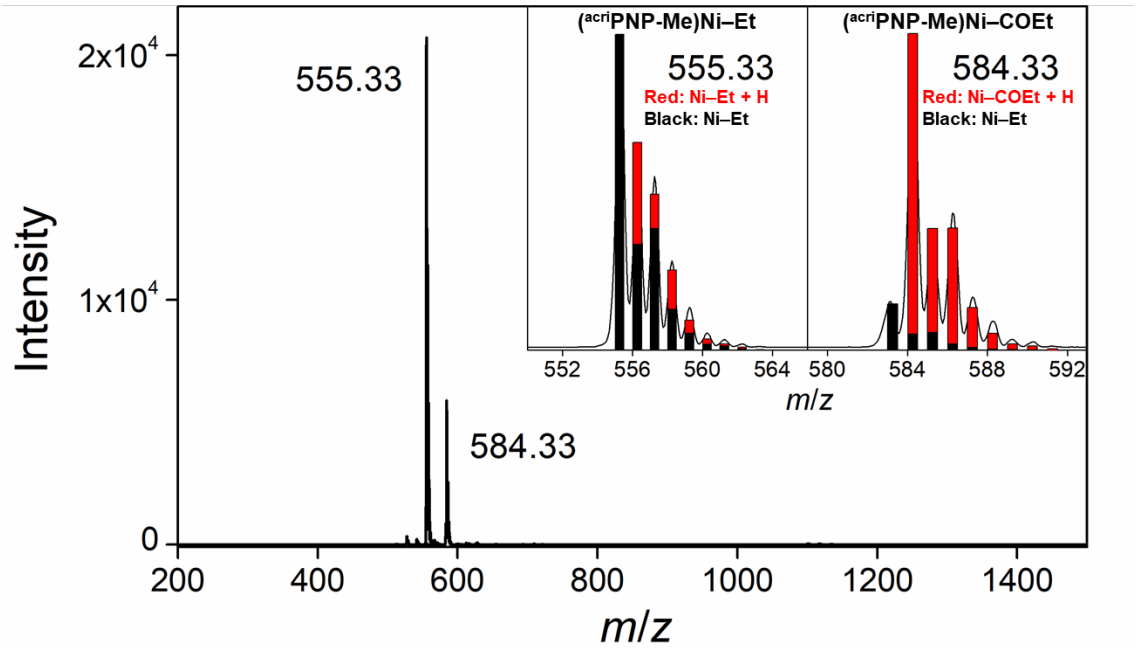

Figure S55. ESI-MS spectrum obtained from the solution of a reaction of **3'** and ^{t}BuI under N_2 atmosphere in THF**;** the peak at m/z = 612.25 correspond to $[(^{acri}PNP\text{-}Me)Ni–CO^tBu + H]^+$ (calcd. m/z 612.30) and the peak at m/z = 554.25 correspond to $[(^{acri}PNP\text{-}Me)Ni–CO]^+$ (calcd. m/z 554.23).

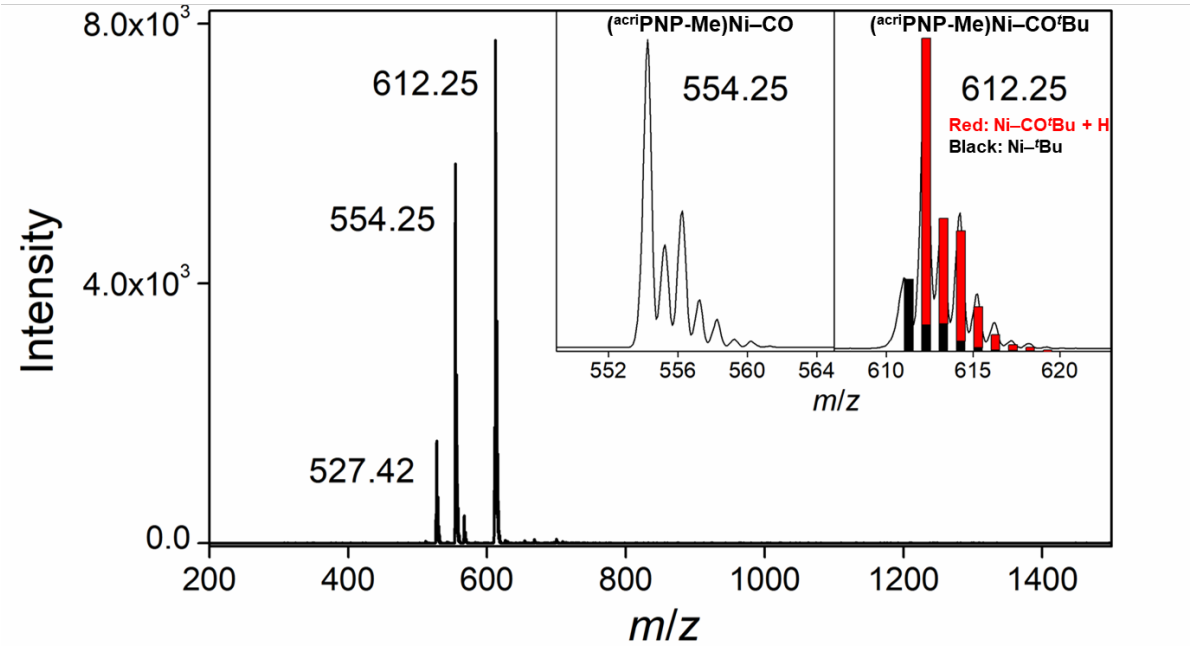

Table S5. Mulliken spin density of (PNP)Ni–CO, (^{acri}PNP-Ph)Ni–CO (**2**), (^{acri}PNP-Me)Ni–CO (**2'**). Lobal representations correspond to the spin density by the number with 0.004 isocontours. Hydrogen atoms are omitted for clarity.

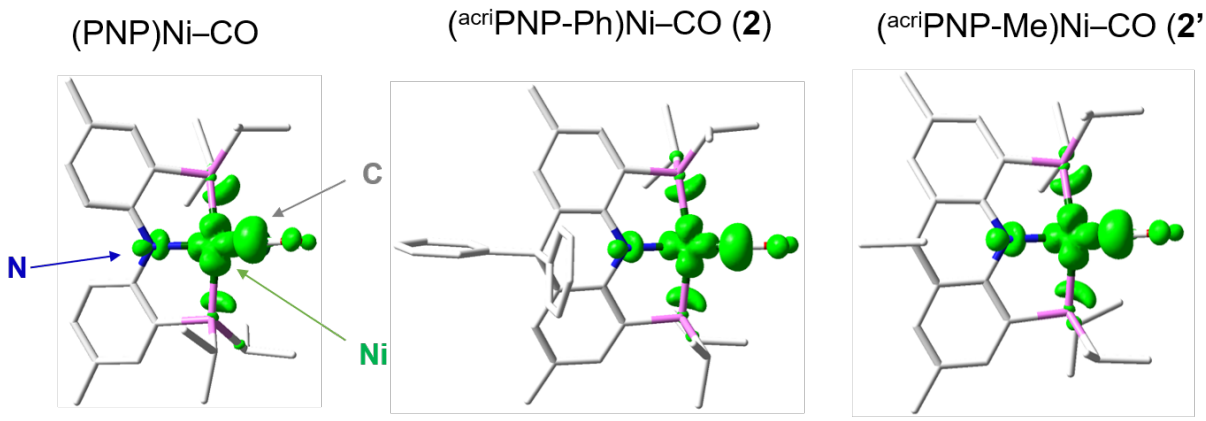

Ni	**68.5%**	**68.03%**	**67.5%**
C	**8.60%**	**9.02%**	**8.27%**
P	**6.30%**	**6.27%**	**6.71%**
P	**6.60%**	**6.18%**	**6.38%**
N	**3.51%**	**4.26%**	**5.46%**

Figure S56. DFT calculated SOMO of (PNP)Ni–CO, (^{acri}PNP-Ph)Ni–CO (**2**), (^{acri}PNP-Me)Ni–CO (**2'**). Hydrogen atoms are omitted for clarity. Lobal representations are described with 0.06 isovalue.

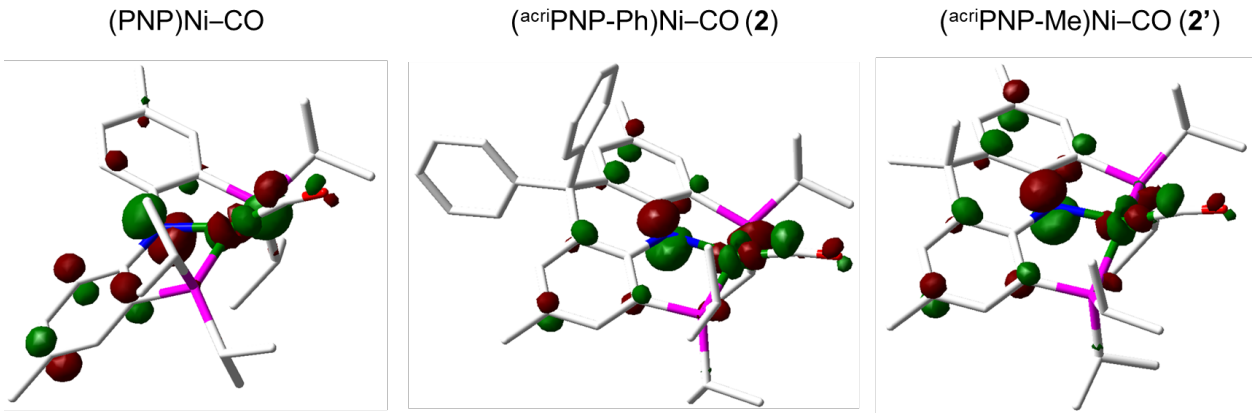

Figure S57. DFT calculated HOMO of anionic portions of [Na][(PNP)Ni–CO], [Na][(^{acri}PNP-Ph)Ni–CO] (**3**), [Na][(^{acri}PNP-Me)Ni–CO] (**3'**). Hydrogen atoms are omitted for clarity. Lobal representations are described with 0.06 isovalue.

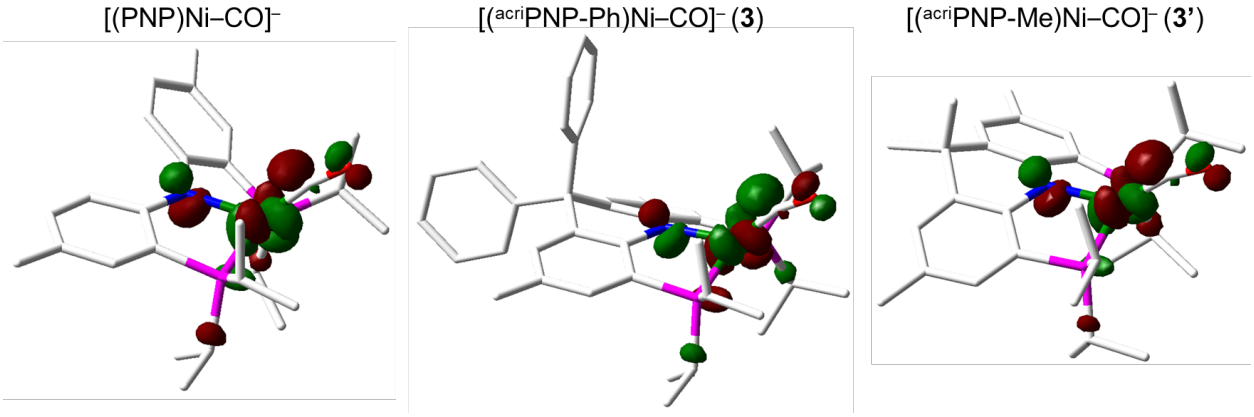

Coordinates are in xyz-file format with charge/multiplicity in parenthesis in the comment line.

(PNP)Ni–CO (0/2)

Ni	-0.01364	-1.11079	-0.37066
P	2.27706	-0.84982	-0.26076
P	-2.13045	-0.84359	0.56156
N	-0.04064	0.91507	-0.35135
C	-0.11679	-2.75740	-1.08467
C	2.34513	0.94310	0.07730
C	3.16073	-1.13998	-1.89890
C	3.35145	-1.67521	1.03819
C	-2.45392	0.80216	-0.18443
C	-2.27828	-0.61951	2.42825
C	-3.59635	-1.91517	0.08771
C	-1.27761	1.50482	-0.58445
C	1.08613	1.62570	0.00000
O	-0.12413	-3.88572	-1.32419
C	3.51139	1.61831	0.47232
H	3.06632	-2.23086	-2.04545
C	2.39166	-0.44587	-3.03161
C	4.64701	-0.76751	-1.92331
H	4.34055	-1.18722	1.00814
C	3.53307	-3.16924	0.73464
C	2.74571	-1.46151	2.43133
C	-3.72699	1.33979	-0.42289
H	-2.10842	-1.63810	2.81958
C	-1.14544	0.27669	2.94466
C	-3.64798	-0.12760	2.90812
H	-4.50659	-1.40075	0.43931
C	-3.51467	-3.28189	0.78434
C	-3.69216	-2.07411	-1.43647
C	-1.47490	2.73124	-1.26961
C	1.10385	2.99724	0.39058
H	4.45241	1.06380	0.53172
C	3.51824	2.97484	0.81681
H	2.84127	-0.69926	-4.00591
H	2.42562	0.65029	-2.92227
H	1.33457	-0.75015	-3.05335
H	5.08397	-1.04005	-2.89892
H	5.22987	-1.28664	-1.14738
H	4.79026	0.31639	-1.79100
H	4.12978	-3.64374	1.53114
H	4.05575	-3.34791	-0.21704

H	2.56254	-3.69065	0.69175
H	3.39898	-1.90602	3.20033
H	1.75768	-1.94423	2.51012
H	2.62296	-0.39423	2.66885
H	-4.61322	0.78385	-0.10391
C	-3.91016	2.56785	-1.07406
H	-1.16827	0.31321	4.04641
H	-1.25022	1.30882	2.57364
H	-0.15763	-0.09232	2.63315
H	-3.65405	-0.05353	4.00875
H	-4.46733	-0.80444	2.62231
H	-3.87587	0.87324	2.50798
H	-4.36682	-3.91036	0.47728
H	-3.54633	-3.20034	1.88133
H	-2.59165	-3.81824	0.51017
H	-4.59021	-2.65931	-1.69497
H	-2.81959	-2.60993	-1.84119
H	-3.76296	-1.10493	-1.95165
H	-0.61048	3.27685	-1.65052
C	-2.75074	3.23913	-1.50207
H	0.17249	3.56211	0.41450
C	2.27607	3.63666	0.77729
C	4.78303	3.69516	1.21811
C	-5.28439	3.14576	-1.31393
H	-2.84933	4.18432	-2.04602
H	2.22230	4.68997	1.07302
H	4.65113	4.25885	2.15716
H	5.09917	4.42615	0.45259
H	5.61744	2.99207	1.36373
H	-5.42265	3.44171	-2.36733
H	-5.45662	4.05089	-0.70526
H	-6.07519	2.42341	-1.06103

(^{acri}PNP-Ph)Ni–CO (**2**)

(0/2)

Ni	2.27878	-0.01060	0.40536
P	2.21162	2.22550	-0.18487
P	2.14208	-2.23979	-0.21549
N	0.31041	0.02548	0.03210
O	4.77907	-0.09954	1.94567
C	-2.38102	2.56446	-0.31690
H	-3.47154	2.61475	-0.36269
C	-1.65424	3.76586	-0.37885
C	-0.25929	3.67493	-0.30080
H	0.32917	4.59535	-0.34377
C	-1.77519	1.31558	-0.16062
C	-0.35579	1.23034	-0.08685
C	2.78938	2.69841	-1.91849
H	3.86570	2.45195	-1.89151
C	-2.74984	-0.21015	1.60776
C	0.39216	2.44075	-0.17522
C	-2.38661	-2.27644	-1.05922
H	-3.47065	-2.27905	-1.19637
C	2.88352	3.56057	0.94797
H	2.49401	4.52374	0.57663
C	-2.36203	5.09378	-0.51131
H	-3.00327	5.12440	-1.40864
H	-1.64525	5.92560	-0.58441
H	-3.01788	5.29502	0.35333
C	-1.78296	-1.14226	-0.51342
C	-2.67124	0.84184	2.53493
H	-2.46573	1.85508	2.18886
C	-0.29065	-3.43209	-1.15745
H	0.28714	-4.32919	-1.39578
C	2.63516	4.17289	-2.30713
H	1.57535	4.46564	-2.36476
H	3.07462	4.33936	-3.30528
H	3.14269	4.85579	-1.60961
C	-0.36634	-1.11520	-0.34739
C	-2.59106	0.03179	0.06960
C	0.35997	-2.31179	-0.62136

C	-3.97330	0.15037	-0.61487
C	-4.03000	0.32064	-2.01232
H	-3.10038	0.35208	-2.58499
C	2.39204	-3.41547	1.23984
H	3.45704	-3.26597	1.49361
C	-1.66634	-3.43123	-1.41537
C	4.41783	3.60567	0.90192
H	4.85968	2.65251	1.23268
H	4.78963	4.39472	1.57632
H	4.80409	3.82592	-0.10480
C	3.05367	-3.04165	-1.64740
H	2.62336	-4.04919	-1.77772
C	2.11904	1.77961	-2.94803
H	2.22539	0.71877	-2.67942
H	2.57101	1.92893	-3.94237
H	1.04240	1.99819	-3.03260
C	-5.18570	0.12085	0.08778
H	-5.18473	-0.00382	1.17091
C	-5.24812	0.45012	-2.67937
H	-5.25971	0.57949	-3.76498
C	2.36919	3.35435	2.37933
H	1.26981	3.35102	2.42422
H	2.73162	4.16708	3.03035
H	2.72800	2.40220	2.80177
C	-2.36327	-4.62056	-2.03294
H	-3.25729	-4.91376	-1.45755
H	-1.69668	-5.49475	-2.08570
H	-2.70510	-4.40378	-3.06048
C	1.55402	-2.94769	2.43822
H	1.74363	-1.89265	2.68569
H	1.79420	-3.55465	3.32670
H	0.47606	-3.05833	2.23855
C	-2.85166	0.61907	3.90552
H	-2.78117	1.46022	4.60052
C	4.54964	-3.18181	-1.33275
H	5.00972	-2.19783	-1.14337
H	5.07325	-3.63470	-2.19083
H	4.74163	-3.81954	-0.45678
C	-6.45172	0.41576	-1.96286
H	-7.40783	0.51713	-2.48276
C	3.73421	-0.06223	1.45859
C	-6.41325	0.25193	-0.57810
H	-7.34209	0.22515	-0.00208
C	-3.01275	-1.49856	2.10801
H	-3.07644	-2.34307	1.42060
C	-3.11519	-0.66607	4.38460
H	-3.25259	-0.84219	5.45459
C	2.83102	-2.24982	-2.94098
H	1.76262	-2.12770	-3.17405
H	3.30460	-2.77239	-3.78844
H	3.28312	-1.24754	-2.87371
C	2.16303	-4.90353	0.95350
H	1.10874	-5.10879	0.71119
H	2.41368	-5.49556	1.84993
H	2.78475	-5.28231	0.12858
C	-3.19679	-1.72553	3.47504
H	-3.40193	-2.73917	3.83000

(^{acri}PNP-Me)Ni–CO (**2'**)

(0/2)

Ni	0.09188	-1.30837	-0.59178
P	-2.10064	-1.37166	0.14797
P	2.27526	-1.02783	0.12133
N	-0.06593	0.65673	-0.30231
C	0.20064	-2.75980	-1.64116
C	-2.44455	0.42722	0.09554
C	-2.40650	-1.92498	1.92697
C	-3.46292	-2.17226	-0.86267
C	2.31187	0.80659	0.14117
C	2.64784	-1.55867	1.89779
C	3.75012	-1.50963	-0.93892

C	1.05749	1.43550	-0.10501
C	-1.30382	1.24781	-0.13633
O	0.28124	-3.79208	-2.15058
C	-3.70779	1.00367	0.29491
H	-2.11436	-2.98997	1.90540
C	-1.44172	-1.18980	2.86633
C	-3.85192	-1.82478	2.42618
H	-4.42339	-1.83742	-0.43504
C	-3.39413	-3.70333	-0.76952
C	-3.39277	-1.69441	-2.31954
C	3.45832	1.57886	0.37965
H	1.98558	-0.87667	2.45977
C	4.08405	-1.33242	2.38369
C	2.17316	-2.99449	2.17207
H	4.63869	-1.03973	-0.48342
C	3.57514	-0.94266	-2.35532
C	3.96849	-3.02878	-0.97632
C	1.00496	2.86139	-0.12159
C	-1.48077	2.66282	-0.16407
H	-4.57848	0.36074	0.44971
C	-3.88642	2.39066	0.30377
H	-1.68614	-0.11709	2.92709
H	-0.39869	-1.27863	2.52985
H	-1.50960	-1.60778	3.88415
H	-3.92211	-2.24432	3.44412
H	-4.56199	-2.37966	1.79494
H	-4.18652	-0.77738	2.48030
H	-4.19785	-4.15250	-1.37615
H	-3.51701	-4.07025	0.26081
H	-2.43569	-4.08731	-1.15372
H	-2.44571	-1.99615	-2.79484
H	-3.47625	-0.60003	-2.39696
H	-4.21679	-2.13850	-2.90224
H	4.42091	1.08601	0.54057
C	3.40806	2.97588	0.41532
H	4.15934	-1.59064	3.45360
H	4.40118	-0.28550	2.27681
H	4.80596	-1.96729	1.84578
H	2.80776	-3.74179	1.67130
H	1.13881	-3.15311	1.83150
H	2.21280	-3.20282	3.25425
H	4.45477	-1.19263	-2.97142
H	3.46537	0.15177	-2.35122
H	2.68770	-1.37060	-2.84917
H	3.08054	-3.55740	-1.35792
H	4.21275	-3.44496	0.01154
H	4.80952	-3.26691	-1.64852
C	2.16450	3.58483	0.16058
C	-0.29135	3.52688	-0.60469
C	-2.75052	3.19065	0.07538
C	-5.24098	3.01964	0.53097
C	4.63483	3.81153	0.69586
H	2.12571	4.67637	0.15278
C	-0.41628	4.98188	-0.12207
C	-0.26452	3.53049	-2.16188
H	-2.88835	4.27402	0.05606
H	-6.01997	2.25576	0.67531
H	-5.54688	3.65080	-0.32122
H	-5.24322	3.67028	1.42260
H	4.82949	4.53643	-0.11302
H	5.53252	3.18418	0.80458
H	4.52472	4.39724	1.62520
H	-0.44048	5.04667	0.97697
H	-1.32888	5.45194	-0.51521
H	0.42266	5.59241	-0.48504
H	0.59318	4.11595	-2.53141
H	-1.19094	3.97359	-2.56236
H	-0.17612	2.50730	-2.55769

References

(1) Yoo, C.; Lee, Y. A T-shaped Nickel(I) Metalloradical Species. *Angew. Chem. Int. Ed.* **2017**, *56*, 9502–9506.

(2) Sahoo, D.; Yoo, C.; Lee, Y. Direct CO_2 Addition to a Ni(0)–CO Species Allows the Selectiv e Generation of a Nickel(II) Carboxylate with Expulsion of CO. *J. Am. Chem. Soc.* **2018**, *14 0*, 2179–2185.

(3) (a) You, F.; Zhai, J.; So, Y.-E.; Shi, X. Rigid Acridane-Based Pincer Supported Rare-Earth Complexes for *cis*-1,4-Polymerization of 1,3-Conjugated Dienes. *Inorg. Chem.* **2021**, *60*, 17 97–1805. (b) Park, I. S.; Matsuo, K.; Aizawa, N.; Yasuda, T. High-Performance Dibenzohet eraborin-Based Thermally Activated Delayed Fluorescence Emitters. *Adv. Funct. Mater.* **201 8**, *28*, 1802031.

(4) Sheldrick, G. M. SHELXTL. Version 6.1; Bruker AXS, Inc.: Madison, WI, 2000.

(5) Stoll, S.; Schweiger, A. Easyspin, a comprehensive software package for spectral simulation and analysis in EPR. *J. Magn. Reson.* **2006**, *178*, 42–55.

(6) Kohn, W.; Sham, L. J. Self-Consistent Equations Including Exchange and Correlation Effect s. *Phys. Rev.* **1965**, *140*, A1133–A1138.

(7) Wiegend, F. Accurate Coulomb-fitting basis sets for H to Rn. *Phys. Chem. Chem. Phys.* **200 6**, *8*, 1057–1065.

(8) Weigend, F.; Ahlrichs, R. Balanced basis sets of split valence, triple zeta valence and quadru ple zeta valence quality for H to Rn.: Design and assessment of accuracy. *Phys. Chem. Chem. Phys.* **2005**, *7*, 3297–3305.

(9) Frisch, M. J.; Trucks, G. W.; Schlegel, H. B.; Scuseria, G. E.; Robb, M. A.; Cheeseman, J. R.; Scalmani, G.; Barone, V.; Petersson,G. A.; Nakatsuji, H.; Li, X.; Caricato, M.; Marenich, A. V.; Bloino, J.; Janesko, B. G.; Gomperts, R.; Mennucci, B.; Hratchian, H. P.; Ortiz, J. V.; Izmaylov, A. F.; Sonnenberg, J. L.; Williams-Young, D.; Ding, F.; Lipparini, F.; Egidi, F.; Goings, J.; Peng, B.; Petrone, A.; Henderson, T.; Ranasinghe, D.; Zakrzewski, V. G.; Gao, J.; Rega, N.; Zheng, G.; Liang, W.; Hada, M.; Ehara, M.; Toyota, K.; Fukuda, R.; Hasegawa, J.; Ishida, M.; Nakajima, T.; Honda, Y.; Kitao, O.; Nakai, H.; Vreven, T.; Throssell, K.; Mo ntgomery, J. A., Jr.; Peralta, J. E.; Ogliaro, F.; Bearpark, M. J.; Heyd, J. J.; Brothers, E. N.; Kudin, K. N.; Staroverov, V. N.; Keith, T. A.; Kobayashi, R.; Normand, J.; Raghavachari, K.; Rendell, A. P.; Burant, J. C.; Iyengar, S. S.; Tomasi, J.; Cossi, M.; Millam, J. M.; Klene, M.; Adamo, C.; Cammi, R.; Ochterski, J. W.; Martin, R. L.; Morokuma, K.; Farkas, O.; Fore sman, J. B.; Fox, D. J. *Gaussian 16*. Revision B.01; Gaussian, Inc.: Wallingford CT, 2016.

(10) Cossi, M.; Rega, N.; Scalmani, G.; Barone, V. Energies, structures, and electronic propert ies of molecules in solution with the C-PCM solvation model. *J. Comput. Chem.* **2003**, *24*, 6 69–681.

(11) Falivene, L.; Cao, Z.; Petta, A.; Serra, L.; Poater, A.; Olivia, R. Scarano, V.; Cavallo, L. Towards the online computer-aided design of catalytic pockets. *Nat. Chem.* **2019**, *11* (10), 872–879.

(12) (a) Guzei, I. A.; Wendt, M. *Program Solid-G*, 2004. (b) Guzei, I. A.; Wendt, M. An improved method for the computation of ligand steric effects based on solid angles. *Dalton Trans.*, **2006**, 3991–3999.
(13) Killian, L.; Bienenmann R. L. M.; Broere, D. L. J. Quantification of the Steric Properties of 1,8-Naphthyridine-Based Ligands in Dinuclear Complexes. *Organometallics*, **2023**, *42*, 27–37.
(14) Yoo, C.; Oh, S.; Kim, J.; Lee, Y. Transmethylation of a four-coordinated nickel(I) monocarbonyl species with methyl iodide. *Chemical Science* **2014**, 5 (10), 3853–3858.